Ventricular ELC Structural Changes induced by Skeletal RLC and an A57G cardiomyopathy mutation

A DISSERTATION

SUBMITTED TO THE FACULTY OF THE GRADUATE SCHOOL

OF THE UNIVERSITY OF MINNESOTA

BY

Shan Zhong

IN PARTIAL FULFILLMENT OF THE REQUIREMENTS

FOR THE DEGREE OF

Masters of Science

Acknowledgements

Doing this research has had a big impact on me. I would like to thank to all the people who have supported and helped me throughout this period.

First, I would like to express my sincere gratitude to my advisor Dr. Osha Roopnarine for the help that she gave me during the last year and a half, not only in the scientific area, but also on a personal level. Her guidance is always important for me and supported me through all the time of research and writing of this thesis.

Besides my advisor, I would like to thank my other thesis committee members: Dr. David Odde (BME) and Dr. David D. Thomas (BMBB), for their time for reviewing my thesis and my oral defense.

I would like to thank my parents and my husband for the spiritual and financial support of me while they are away distantly in China.

Abstract

Time-resolved fluorescence quenching measurements were used to measure the conformational changes in the ventricular essential light chain (vELC) for two specific aims. First, is to investigate whether the interactions between cardiac vELC and the ventricular regulatory light chain (vRLC) are isoform-specific, and second, is to determine the conformational effects of the A57G-vELC cardiomyopathy mutation on the ELC structure. Both the ELC and the RLC play essential roles in cardiac muscle contraction, and the specific interactions between ELC and RLC of scallop and smooth muscle are important for the regulation of contraction. The effect of different isoforms of RLC on vELC aids us to investigate the specific requirement of certain RLC isoforms in cardiac muscle. Familial hypertrophic cardiomyopathy (FHC) is a human cardiac disease in which the left ventricle and inter-ventricular septum of the myocardium is hypertrophied. A57G is an ELC mutation that causes FHC, and occurs in the middle of the first α-helix in ELC. In this study, a single cysteine was engineered with ELC at C81 for labeling with a fluorescent probe called IAEDANS. The endogenous RLC and ELC were removed from skinned rabbit psoas muscle fibers. For the first experimental goal, labeled rat wildtype vELC with either rat wildtype vRLC or rabbit skeletal rRLC were exchanged back into the fibers, which were subsequently named as the WT and the rRLC. For the second experimental purpose, either labeled rat wildtype vELC or labeled A57G vELC with rat wildtype vRLC were exchanged back on the fibers and these were subsequently named as the WT and the A57G. The time-resolved fluorescence quenching experiments were performed in rigor, relaxation and contraction solutions, and the quenching of the lifetimes of the probe IAEDANS, was determined as a function of [Acrylamide]. The existence of

rRLC and A57G mutation caused the τ_0 (fluorescence lifetime in the absence of the quencher) of the rRLC and the A57G to be shorter than the WT, respectively. The Stern-Volmer constants for the rRLC and the A57G were also higher to different extents compared to the WT in all solutions, suggesting that the WT has a more closed configuration in which the probe is more buried and less exposed to the solvent. These indicated that both rRLC and A57G could induce ELC conformational changes that may open the domain. The powerstroke during contraction caused less conformational change due to the existence of the skeletal RLC; this suggested that the interaction between RLC and ELC could affect force generation. A potential reason for this change is the different amino acids in the sequence between rRLC and vRLC linker area for the c-terminal domain. The Ksv constants for A57G in states were similar to each other. It is possible that the A57G cardiomyopathy mutation disrupted the helix structure so that the labeled site in vELC were constantly open.

Table of Contents

Abbreviations

A57G A57G-vELC and vRLC reconstituted muscle fiber
ALC1, atrial myosin essential light chain, MYL-4
ALC2, atrial myosin regulatory light chain, MYL-7
DTNB, dithioiobis-nitrobenzoiciacid
EF-hand, Ca^{2+} -binding helix-loop-helix motif
ELC, myosin essential light chain
FHC, familial hypertrophic cardiomyopathy,
LC, light chain
MHC, myosin heavy chain, α–MHC (MYH6) β–MHC (MYH7)
MLC, myosin light chain
MyBP-C, myosin-binding protein-C
RLC, myosin regulatory light chain
rRLC, vELC and rabbit RLC reconstituted muscle fiber
S1, myosin subfragment-1
SCD, sudden cardiac death
SDS-PAGE, sodium dodecylsulfate polyacrylamide gel electrophoresis
SR, sarcoplasmic reticulum,
Tn, troponin complex
V1, ventricular (αα)-MHC myosin
V2,ventricular (αβ)–MHC myosin
V3, ventricular (αα)–MHC myosin
VLC1 ventricular myosin essential light chain, MYL-3
VLC2, ventricular myosin regulatory light chain, MYL-2
WT, vELC and vRLC reconstituted muscle fiber.

Figure List

Chapter 1 Introduction

1.1 Cardiac Muscle contraction

Muscle contraction is a well-understood movement of which animals are capable (Alberts, Bray et al. 1994). Muscle cells evolved with the specialized ability to contract. In vertebrates, there are three types of muscle cells: skeletal, smooth and cardiac muscle cells. Running, walking, and other physical excises all depend on skeletal muscle contraction, while heart pumping and the movement of food through the digestive tract relies on involuntary cardiac and smooth muscle contractions, respectively. Both the skeletal and cardiac muscle tissues are striated (Alberts, Bray et al. 1994), but the cardiomyocytes are of the branched variety, in contrast to the skeletal muscles that have long uniform fibers (Lodish, Berk et al. 2000). The cardiac muscle is a specialized form of striated muscle found in the heart (Alberts, Johnson et al. 2002). The mammalian heart regulates the supply of blood to two separate circulation circuits to provide efficient oxygen and nutrients to the whole body (Furtado, Costa et al. 2016). In an average human lifespan, the cardiac muscle contracts about 3 billion times (Alberts, Bray et al. 1994).

The cardiomyocytes contain one single nucleus and are separated by the intercalating discs (Figure 1). These discs are the regions where adjacent cardiomyocytes interlock and permit an action potential to spread rapidly through the chain (Alberts, Bray et al. 1994). The connection of cardiac muscle cells by the intercalated discs allows cardiac tissue to contract in a synchronized manner (Alberts, Bray et al. 1994). The cardiac fiber, like the skeletal fiber, is also composed of myofibrils, which are actin- and myosin-based contractile units. Each myofibril consists

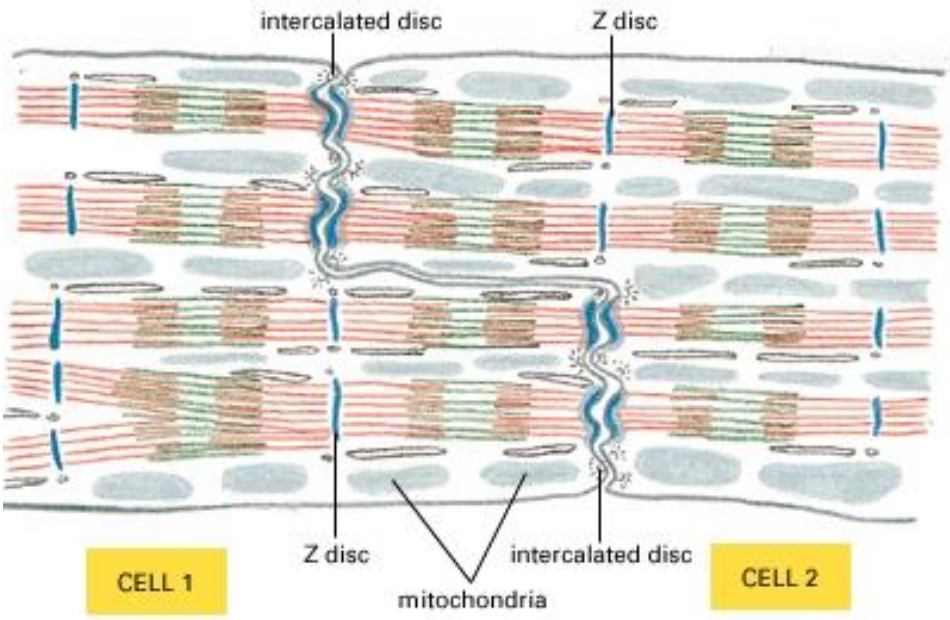

Figure 1. Schematic diagram of heart muscle showing two cells joined end to end by specialized junctions known as intercalated discs.
The cardiomyocytes are separated by intercalating discs. Adapted from (Alberts, Bray et al. 1994).

of contractile building blocks, or sarcomeres (Alberts, Bray et al. 1994) and each sarcomere is 2-μm long (Spudich 2014).

Each sarcomere contains precisely assembled filaments that are parallel to each other and partly overlap (Figure 2, top). The thin filaments are formed from actin as well as other proteins (troponin complex and tropomyosin) and are attached to the Z discs at either end of the sarcomere. The cardiac thick filaments are polymers of the atrial (α or V1) myosin and ventricular (β or V3) myosin.

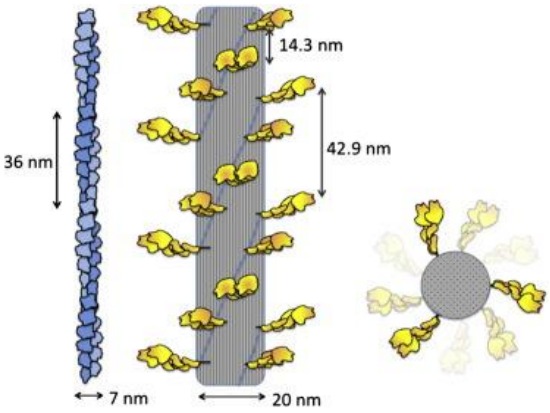

Figure 2. Structures of the actin filament, myosin thick filament (Spudich 2014).
Actin is single-start left-handed helix, each twist with a pseudo-repeat of 36nm. Myosin filament is about 3 times thicker with a three-start right-handed helix. The end view is on the right.

The thick filaments are bipolar and the tails pack into a cylindrical backbone with the heads projecting out laterally (Figure 2). Each cardiac thick filament consists of a three-

start right-handed helical array of myosin heads (Spudich 2014). They form either homodimers or heterodimers in the cardiac cells. The contractions occur when thick and thin filaments slide past each other (Figure 2, bottom). An action potential triggers the sarcoplasmic reticulum (SR) to release Ca^{2+}, which triggers the contraction by exposing the myosin-binding site to the actin. The contraction is driven by a molecular motor, myosin. The hydrolysis of ATP by the myosin head domain provides the energy for muscle contraction.

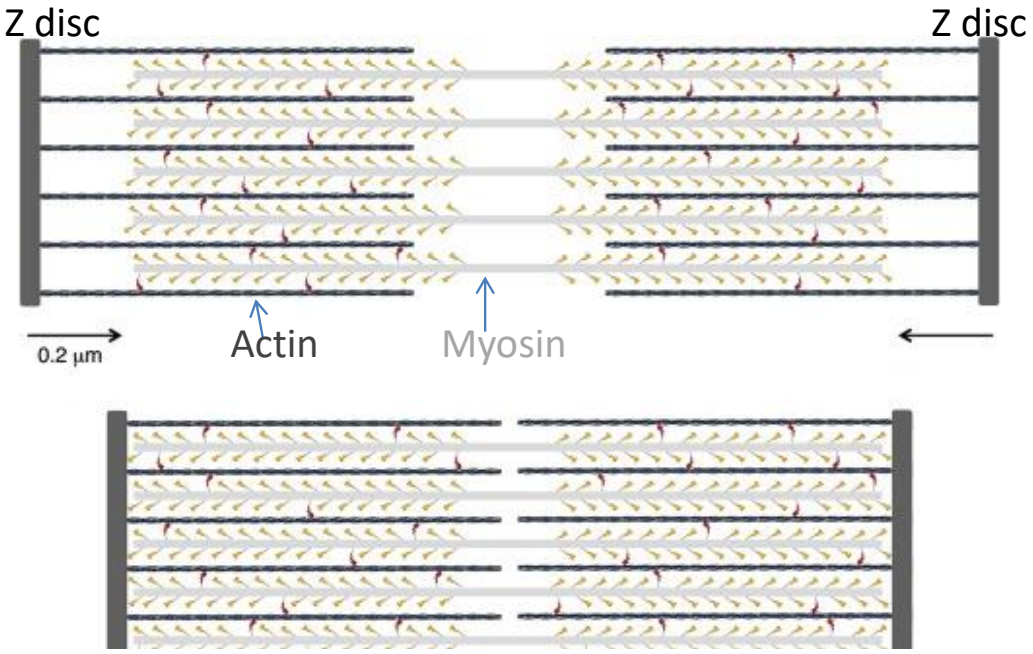

Figure 3. Structure of Sarcomere. (Spudich 2014).
Top: resting state
Bottom: contracting state

1.2 Myosin Structure

The myosin muscle motor is a hexametric protein, which is 520kDa. The myosin consists of two coiled-coil myosin heavy chains (MHC) of around 220kDa (1930-1940 amino acid residues) and 2 pairs of light chains (LC), which are known as the regulatory

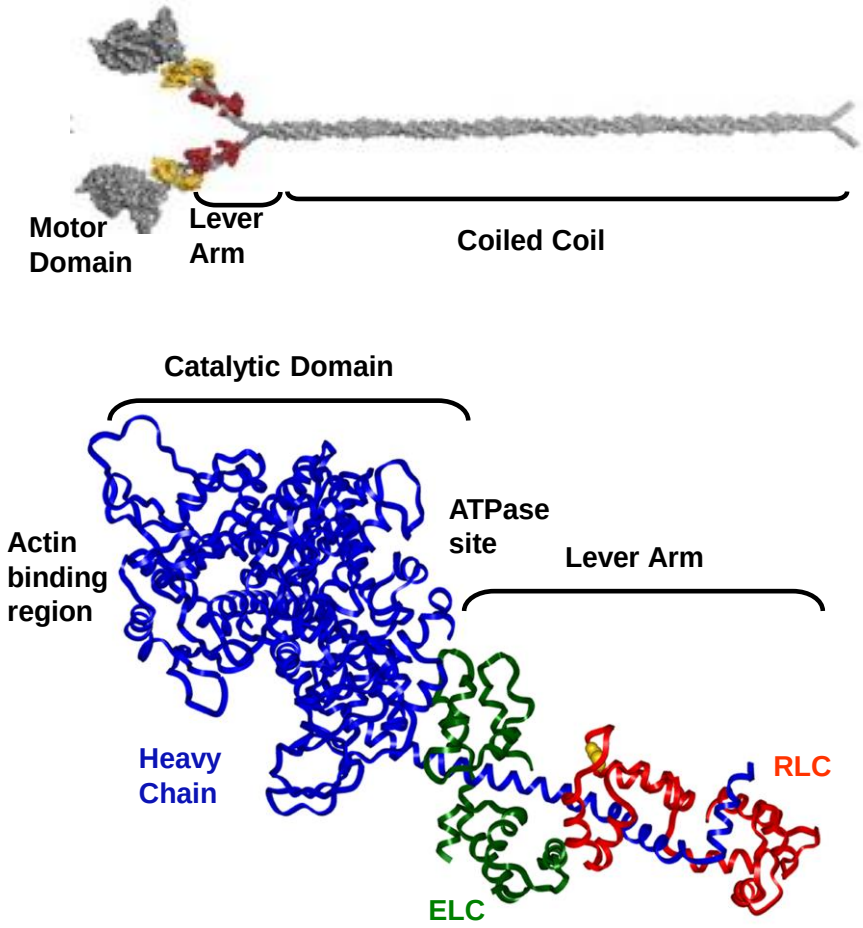

Figure 4. Structure of myosin.
Top: Myosin molecule showing two motor domains, teo lever arms, and a long tail. Bottom: Schematic representation of the myosin head with ELC (green) and RLC (red) binding to the lever arm (Rayment, Rypniewski et al. 1993). (NCBI accession no. NP_001013415. The ATP-binding site, actin-binding site, converter domain (Hernandez, Jones et al. 2007) and the lever arm were labeled.

light chain (RLC) and the essential light chain (ELC) (Muthu, Wang et al. 2011). Myosin can be digested into heavy meromyosin and light meromyosin. There are three major domains in myosin: the motor domain and the lever arm domain are in S1, and the other domain is the tail region (Sweeney and Houdusse 2010) (Figure 4). A

converter subdomain is formed by the C-terminal sequence of the motor domain, which can amplify the conformational change of the motor domain and convert the changes to the lever arm (Sweeney and Houdusse 2010). The lever arm domain contains two IQ motifs (IQxxxRGxxxR) to which the ELC and RLC bind (Hernandez, Jones et al. 2007). The formation of the tail domain is more variable. It can dimerize into a coiled-coil structure, and the C-terminus region can bind with cargo molecules to mediate the interaction of the cargo molecules and myosin subunits (Sweeney and Houdusse 2010).

1.3 Cardiac myosin heavy chains (MHC), MYH7

There are at least 8 MHC isoforms expressed in mammalian striated muscles: two developmental isoforms which are MHC-embryonic and MHC perinatal, four fast isoforms (MHC-fast 2A, 2B, 2X/D and MHC-extracular), one MHC-slow which is equivalent to the cardiac β-MHC, and one cardiac α-MHC isoform (Vikstrom and Leinwand 1996). In large animals such as rabbits, dogs, pigs, and humans, the β-MHC is the predominant ventricular isoform throughout the adulthood (Kelly and Buckingham 1997; Schaub, Hefti et al. 1998). The mutations in β-MHC can result in familial hypertrophic cardiomyopathy (FHC). This will be discussed later in this section.

1.4 Cardiac light chains

As mentioned before, each myosin head contains one set of MLCs, which contains ELC and RLC. The two LCs are located in a series in which the ELC binds to residues from L783 to M806 and RLC binds to E808 to L842 of MHC (Rayment, Rypniewski et al. 1993). Both ELC and RLC belong to the EF-hand protein superfamily, a diverse superfamily of calcium sensors and calcium signal modulators (a helix-loop-helix motif) (Kawasaki and Kretsinger 1994). During evolution, all four EF-hand domains of the vertebrate muscle myosin ELC lost the ability to bind Ca^{2+}, but RLC has the first EF-

domain left to be able to bind either Ca^{2+} or Mg^{2+} (Watterson, Kohler et al. 1979). There is an assumption which proposes that during cardiac muscle contraction, this cite could act as a delayed Ca^{2+} helping the SR to sequester Ca^{2+} during diastole or relaxing (Szczesna 2003; Wang, Xu et al. 2006). The ELC is essential for the stability of the α-helical lever arm and for the movement of the lever arm in cycle. The ELC also plays an important role in transducing the structural arrangement of the motor domain into large movements for force generation (Geeves 2002). There are two isoforms of LCs expressed in the heart: the ALC1 (gene MYL-4) and VLC1 (gene MYL-3) are the atrial and ventricular ELC, respectively, and ALC2 (MYL-7) and VLC2 (MYL-2) correspond to the atrial and ventricular RLC, respectively. The MYL-3 gene is located on chromosome 3p21.2-p21.3. There is much evidence to indicate that the ELC is important in force generation and muscle contraction (Lowey and Trybus 1995; Hernandez, Jones et al. 2007). It contains seven exons, of which six encode a polypeptide with 195 amino acids (Fodor, Darras et al. 1989). The skeletal ELC interacts with actin through its extended N-terminus (Sutoh 1982). Similarly, the cardiac N-terminal ELC extension prepositions the cross-bridge for optimal force production, which is proved by using N-terminally truncated Δ43-ELC (Muthu, Wang et al. 2011). Thus, the cross-bridge properties can be changed significantly due to a slight and subtle alteration in the ELC isoforms. For example, the RLC phosphorylation of Ser15 alternates cardiac muscle contraction (Kamm and Stull 2011).

1.5 Actin-myosin kinetic cycle

The cyclical attachments and detachments between the myosin heads (S1) and actin thin filaments generate the muscle contraction, including the beating of the heart (Geeves and Holmes 2005). The working stroke is powered by ATP hydrolysis in the myosin catalytic domain (Sweeney and Houdusse 2010). The myosin hydrolyzes ATP to provide the energy to detach and attach the actin thin filaments in a cyclical manner (Figure 5). Since the ATP binding pocket is open, the ATP binds to the myosin head domain and induce the detachment of myosin head from the actin filament (Figure 5, Step 1); this is the post-rigor state. The hydrolysis of ATP into ADP and Pi causes a further conformational change, which shift the lever arm of the myosin to point upwards (Figure 5, Step 2). While ADP▪Pi is bound to the myosin, the myosin head reattaches to the actin filament in a weakly binding manner to form a pre-powerstroke state (Figure 5, Step 3a). After the release of Pi, the actin-myosin perform powerstroke (Figure 5, Step 3b) and then the myosin head is strongly bound to actin filament to form a post-

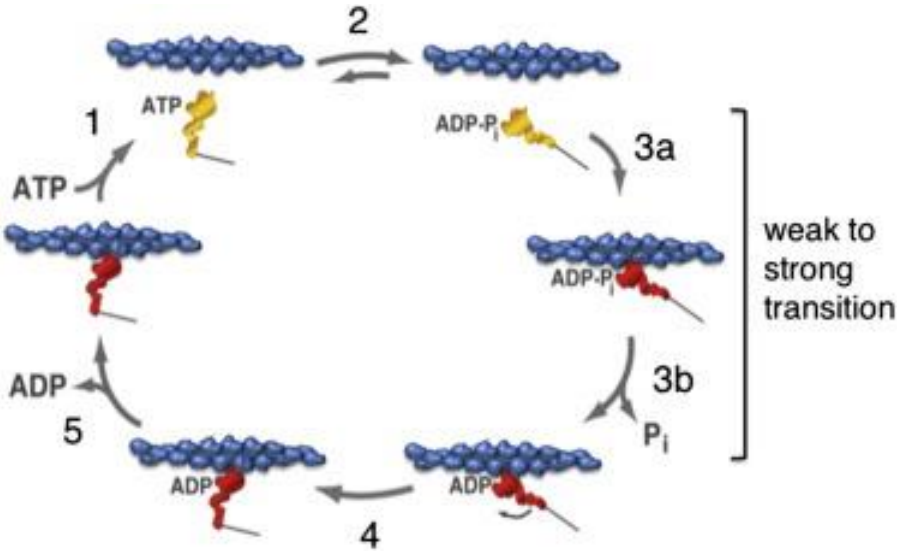

Figure 5. The actomyosin ATPase cycle. Adapted from (Spudich 2014).
Step1: ATP binding to the strongly bound myosin head which dissociated it from actin.
Step2: ATP hydrolysis, which allows a weakly binding of myosin to actin (prepowerstroke).
Step3a and 3b: Rebinding of the head to actin in a strongly bound state is associated with Pi release from the active site
Step4: Powerstroke is performed.
Step5: ADP is released, ATP binding allowed, the cycle continued.

powerstroke state (Figure 5, Step4). The ADP and Pi are released and the actin binding cleft of the cross bridge (motor domain) is closed so that the cross bridge as well as the myosin head are strongly bound to the actin thin filament (Figure 5, Step5).

1.6 Familial hypertrophic cardiomyopathy

Familial hypertrophic cardiomyopathy (FHC) is an inherited disorder and autosomal dominant disease characterized mainly by left ventricular hypertrophy. FHC is also known more simply as cardiomyopathy (HCM). Familial hypertrophic cardiomyopathy affects an estimated 1 in 500 people worldwide. It is one of the most common genetic heart diseases in the United States (Szczesna-Cordary, Guzman et al. 2004; Maron and Maron 2013). This disease is manifested by asymmetric or symmetric cardiac hypertrophy, myocyte/myofibrillar disarray, and fibrosis (Bashyam, Savithri et al. 2003; Kazmierczak, Paulino et al. 2013). The clinical phenotype is highly variable and ranges from a lack of cardiovascular symptoms to shortness of breath, chest pain, syncope, presyncope, or sudden cardiac death (SCD) (Roopnarine 2003; Willott, Gomes et al. 2010; Kazmierczak, Paulino et al. 2013).

FHC is established as a common genetic heart disease in regions including the USA (Maron, McKenna et al. 2003), Europe (Richard, Charron et al. 2003), Japan (Kitaoka, Doi et al. 2003), China, and East Africa (Maron and Maron 2013). There is substantial diversity in the causes of FHC. Most of the mutations (about 90%) of pathogenic mutations altering physical and functional properties of proteins are missense mutations (Maron, Maron et al. 2012). At present, the Online Mendelian Inheritance in Man (OMIM) classifies 32 different FHC phenotypes that are associated with different sarcomeric genes. The earlier report of seven mutations in the β-cardiac myosin heavy-chain gene that are responsible for FHC (Watkins, Rosenzweig et al. 1992) has now been expanded

to more than 11 causative genes with over 1,400 mutations (Maron, Maron et al. 2012; Maron and Maron 2013). Several proteins of the cardiac sarcomere are implicated in the pathogenesis of HCM, leading the current view of FHC as being a "disease of the sarcomere" (Tardiff 2005).

Mutations in the β-myosin heavy-chain (MYH7 gene), regulatory myosin light chain (MYL2 gene), and essential myosin light chain (MYL3 gene) which encoded thick filament, cardiac troponin T (TNNT2), cardiac troponin I (TNNI3), cardiac troponin C (TNNC1), α-tropomyosin (TPM1), and α-cardiac actin (ACTC) which encoded thin filaments, intermediate filament coding gene cardiac myosin-binding protein C (MYBPC3) and Z-disc coding genes α-actinin 2 and myozenin 2 have the strongest evidence for pathogenicity; other genes like α-myosin heavy chain (MYH6), titin (TTN), muscle LIM protein (CSRP3), telethonin (TCAP), vinculin (VCL), calsequestrin (CASQ2) and junctophilin2 (JPH2) have less evidence for pathogenicity (Maron, Maron et al. 2012) (Figure 6). Among these, approximately 70% have mutations in the two genes

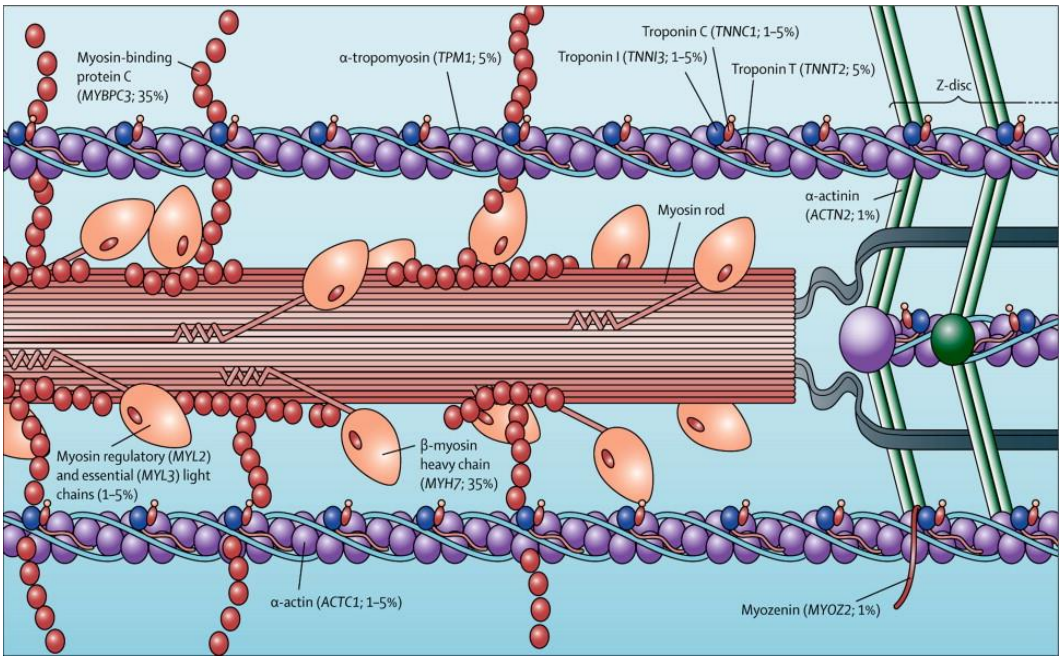

Figure 6. Locations of the genes that cause FHC and the prevalence of each gene are shown in parentheses. Adapted from (Maron and Maron 2013).

(Maron and Maron 2013) MYH7 and MYBPC3, while mutations in TNNT2, TNNI3, ACTC, TPM1, MYL3, and MYL2 collectively account for less than 20% of successfully genotyped cases (Konno, Chang et al. 2010). The locations of genes within the cardiac sarcomere known to cause hypertrophic cardiomyopathy and the percentage of each gene are shown in Figure 6.

1.6.1 FHC-associated ELC mutations

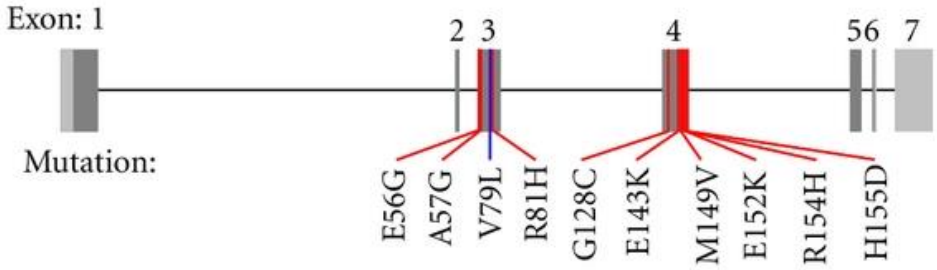

Figure 7. The genomic structure of MYL3 with the known disease-causing mutations is indicated. Adapted from (Andersen, Hedley et al. 2012)

There are ten mutations in the myosin ELC (product of MYL3 gene) that are associated with FHC: E56G, A57G, V79L, and R81H are on exon three and six; while G128C, E143K, M149V, E152K, R154H, and H155D are on exon four (Richard, Charron et al. 2003; Arad, Penas-Lado et al. 2005; Andersen, Hedley et al. 2012; Kazmierczak, Paulino et al. 2013) (Figure 7). All FHC vELC mutations are in highly conserved amino acid residues (Hernandez, Jones et al. 2007). The phenotypes of ELC mutations can vary from FHC with autosomal dominant inheritance, which can result in SCD (A57G and M149) (Lee, Hwang et al. 2001; Arad, Penas-Lado et al. 2005), to

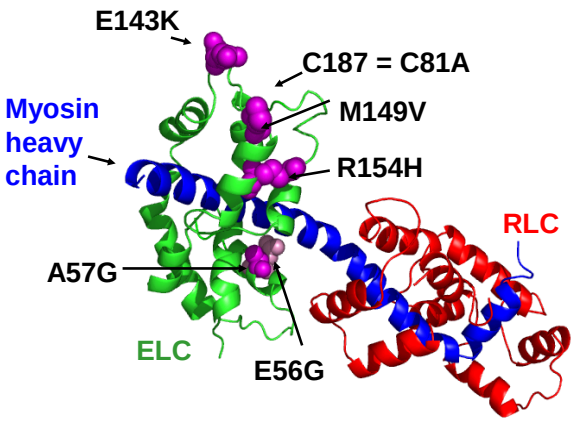

Figure 8: Chicken skeletal crystal structure (Rayment et al, 1993) of the LC binding domain in myosin showing some of the FHC-ELC mutations.

a recessive phenotype; only homozygosity was associated with SCD (Olson, Karst et al. 2002). The three-dimensional structure of five of the ten identified FHC mutations in vELC is demonstrated in Figure 8.

1.6.2 A57G ELC mutation

The amino acid sequence alignment of ventricular ELC from different organisms reveals a high sequence homology among ELC from different species and demonstrates that the A57G-vELC residues of HCELC are highly conserved in all of the presented ELC sequences (Figure 9). The A57G mutation is predicted to be in the α-helix of the first EF-hand domain. For the ELC and its N-terminal molecular interaction with actin, the N-terminal A57G mutation is expected to affect the myosin-actin interaction directly. The ELC-A57G mutation was first found in two unrelated Korean families and one Japanese patient that were found to contain hypertrophic cardiomyopathy (Lee, Hwang et al. 2001). The phenotype of the A57G mutation contains an asymmetric septal hypertrophy (ASH) (Lee, Hwang et al. 2001), post-adolescent phenotypic manifestation, and a high rate of young-age SCD (Hernandez, Jones et al. 2007). Previous research have shown that the A57G mutation causes a tighter packing of the

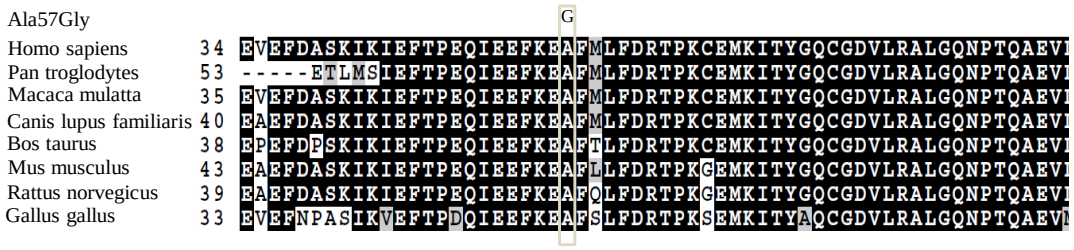

Figure 9. Multiple alignment of regions flanking the mutation in MLC-3 (NCBI accession numbers in parentheses following) showing evolutionary conservation of the mutated region across species. Homo sapiens (Human NP_000249.1), Pan troglodytes (chimpanzee XP_003309811.2), monkey (XP_001113910.1), Canis lupus familiaris (dog XP_005632679.1), Bos Taurus (cattle NP_001069969.2), Mus musculus (house mouse NP_034989.1), Rattus norvegicus (rat NP_036738.1), Gallus gallus (chicken NP_990490.1).

thick filaments sarcomeres (Muthu, Wang et al. 2011); it can also decrease the maximal force generation and increase passive tension when compared to WT-ELC mice (Muthu, Wang et al. 2011; Kazmierczak, Paulino et al. 2013).

1.7 Quenching of fluorescence

Fluorescence quenching is the process that decreases the fluorescence intensity of the sample. Quenching can be achieved through different mechanisms, excited-state reactions, molecular rearrangements, energy transfer, ground-state complex formation, and collisional quenching (Lakowicz 2006). The conformational changes of proteins in complex can be detected through the fluorescence quenching method. Dynamic quenching is based on a non-photochemical reaction that the quencher must diffuse to the fluorophore. Next, the energy of the excitation previously absorbed by the probe must be removed (Lakowicz 2006; Mátyus, Szöllősi et al. 2006). The fluorophores are excited to excited-state, S1; some collide with the quencher molecule and return to ground state, S_0 non-radioactively (Figure 10). In this case, both fluorescence intensity and fluorescence lifetime are affected by the quencher. For a dynamic quenching, the fluorophore and the quencher become a complex in the ground state of the fluorophore, and thus quenching occurs due to a lower population of excited-state fluorophores. The direct physical contact between the probe and the quencher is required for both dynamic and static quenching. Due to the difference of the quenching mechanism for dynamic and static quenching, they can be distinguished by lifetime measurement. Lifetime is also shortened in dynamic quenching because it depopulates the excited state without fluorescence emission; static quenching does not lower the lifetime since observation

is from the fluorescent molecules which are uncomplexed fluorophores that maintained the lifetime without quencher τ_0 (Lakowicz 2006).

The Stern-Volmer equation is a classical analysis used to interpret quenching results (Mátyus, Szöllősi et al. 2006) (Figure 10). This equation is also listed in the methods section (Equation 6). The classical Stern-Volmer plot is suitable for the analysis of quenching data obtained with neutral quenchers such as acrylamide, or charged quenchers such as cesium chloride (Mátyus, Szöllősi et al. 2006). The quenching measurement is also sensitive to pressure and temperature, thus measurement of the quenching of fluorophore must be under controlled experimental conditions. The Stern-Volmer equation is obeyed when a single fluorophore exists in one protein and only one type of quenching occurs (Lakowicz 2006). With multiple fluorophores containing protein, a curvature downwards can be observed as the quencher concentration increases (Lakowicz 2006). If a marked upward curvature is

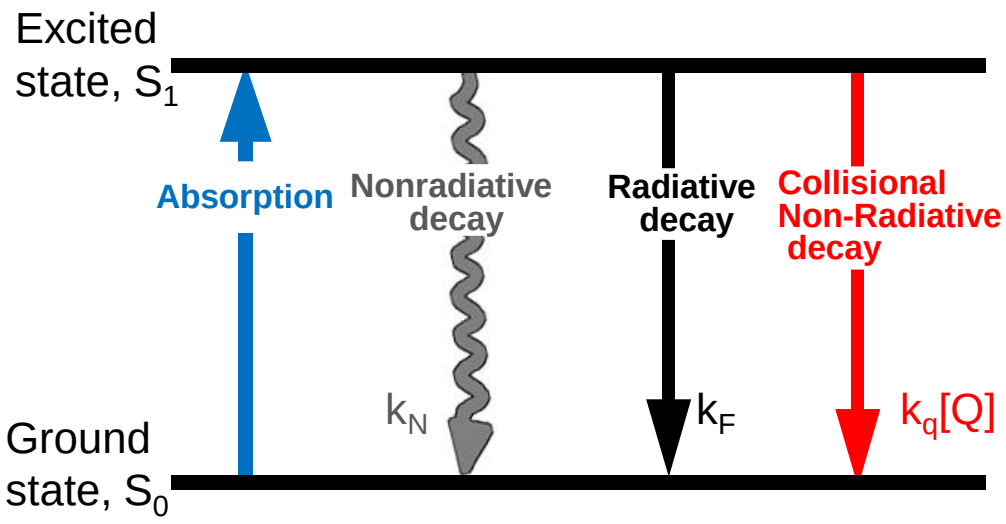

Figure 10. Scheme of Collisional quenching and derivation of Stern-Volmer Equation.
$k=k_N+k_F+k_q[Q]$, quantum yield$=F/F_0=\tau/\tau_0 = k_0 / k = k_0 / (k_0 + k_Q[Q]) = 1 / (1 + k_q[Q] / k_0)$
$F_0/F=1 + k_q[Q] / k$ = Stern-Volmer Equation, which is usually written as $F_0/F/ =\tau_0/\tau=1+Ksv[Q]$, where $Ksv=k_q\tau_0$

observed, this indicates that static quenching as well as collisional quenching is occurring (Bell 1981; Lakowicz 2006).

1.8 Motivation of Research

1.8.1 Optimization of ventricular ELC purification procedure

Protein purification is important when studying the function and structure of a protein and a protein's interaction with other proteins. In order to study the conformational change of myosin by RLC isoforms and FHC-ELC mutation, the purification of wildtype ventricular ELC (WT ELC) and mutant ventricular ELC (FHC-ELC) is essential. The wildtype rat vELC, FHC-ELC and vRLC were expressed in an *Escherichia coli* cell line, called BL21Ai. In order to maximize the yield and minimize the occasional degradation of the protein, the procedure was improved by involving one column chromatography rather than two column chromatography.

In the previous ion exchange chromatography, the ionic strength increases too quickly, which leads to a fast elution of ELC at the beginning of the gradient elution. The high molecular weight impurities were eluted at higher ionic strength compared to the ELC. Thus, the gradient of NaCl was changed from 0mM to 500mM to 0mM to 300mM.

The sodium dodecyl sulfate-polyacrylamide gel electrophoresis (SDS-PAGE) was used to analyze the pooled fractions from the gradient elution. This was done in order to determine the fractions that contain the protein and the purity of the lyophilized final product. Protein concentrations were determined by the Bradford assay (Bio-Rad), using bovine serum albumin as the standard.

1.8.2 Effect of skeletal rRLC on vELC structure

The interaction between scallop ELC and RLC is necessary for the activation of myosin (Xie, Harrison et al. 1994; Himmel, Mui et al. 2009). It is also reported that, in

smooth muscle, the destruction of the RLC/ELC interface can increase the flexibility at the interface and ELC-binding site of the HC and hence inhibit the activation of smooth muscle myosin (Ni, Hong et al. 2012). The dephosphorylated state of myosin (inhibited), which detaches the myosin from actin, is due to an asymmetric intramolecular head-head interaction. Computational modeling suggested that this is achieved by torsional and bending motions about the location of MHC that is between the RLC and ELC, and modification of the relative motions between ELC and RLC can affect the inhibited state (Taylor, Feig et al. 2014). This interaction between myosin heads is also observed in cardiac muscle (Zoghbi, Woodhead et al. 2008), and RLC phosphorylation can occur in cardiac muscle as well (Sweeney, Bowman et al. 1993). Thus, it is reasonable to speculate that ELC and RLC interaction can modify cardiac contraction. In addition, previous reports have shown that substitution of skeletal RLC with ventricular RLC on skeletal skinned muscle fiber increased Ca^{2+} sensitivity to a higher degree than the original unchanged fibers (Roopnarine 2003). In transgenic mice, the expression of skeletal rather than the ventricular RLC isoforms reduced left ventricular contractility and relaxation (Gulick, Hewett et al. 1997). Thus, it is possible that there is an interaction between vELC and vRLC such that skeletal rRLC can perturb this interaction and induce a vELC conformational change in cardiac muscle contraction.

In the present study, the conformational change in ventricular vELC due to different sources of RLC (cardiac vRLC and skeletal RLC) was investigated using dynamic quenching measurement during rigor, relaxation, and

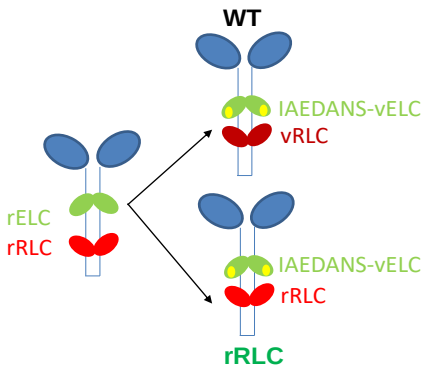

Figure 11. Reconstituted the rRLC. The endogenous skeletal ELC (rELC) was exchanged by fluorescent recombinant vELC, rRLC, and vRLC were exchanged back for two kinds of chimeras which were called the WT and rRLC, respectively.

contraction of muscle fibers. Rat cardiac vELC was used as the background. The amino acid similarity between human vELC and rat vELC is 96%, which makes it a good candidate for studying the conformational effect of ventricular ELC due to different RLC sources. The native ELC of isolated rabbit psoas fibers was substituted by a fluorescently labeled vELC (Figure 11). Rabbit psoas fibers were used instead of cardiac muscle fibers because it is difficult to obtain long, psoas-like fibers from the heart, which has branched fibers. Furthermore, the RLC fiber-extraction procedure used in this present study involved 5,5-dithio-bis- (2-nitrobenzoic acid) (DTNB), which works in fast skeletal fibers (Szczesna, Zhao et al. 1996) but not in soleus or cardiac fibers (Wagner 1982). The fast skeletal RLC contains cysteines that can react with DTNB whereas the vRLC does not, which is likely the reason (Huber, Brunner et al. 1989). The similarity of ELC and RLC binding region of myosin HC of rabbit skeletal and cardiac β-myosin isoforms is 95%, thus the binding of vELC and vRLC to rabbit fast myosin is less possible to be impaired. The C81 site on vELC was labeled with IAEDANS. The dynamic quenching experiment was performed with a range of concentrations of acrylamide (0 M-0.5 M) for the two chimeras (Figure 11, the WT and rRLC). The different lifetimes, Stern-Volmer constants, quenching rate constants derived from the two quenching experiments, proved that conformational change of ELC from rigor, relaxed, and contracted states depend on various sources of RLC.

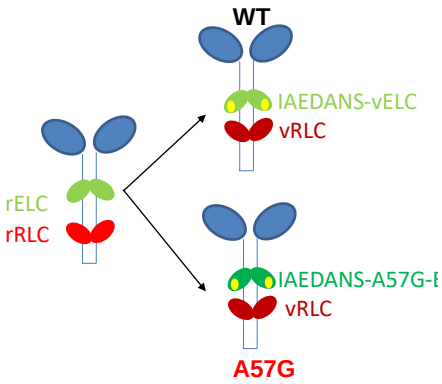

Figure 12. Reconstituted chimera A57G.
The endogenous skeletal ELC (rELC) was exchanged by fluorescent recombinant vELC and A57G-vELC, vRLC were exchanged back for the two kinds of chimeras which were named as the WT and the A57G.

1.8.3 Effect of A57G ELC mutation on ELC structure

My study focused on one of the ELC mutations that cause FHC, A57G-vELC. As mentioned previously in Chapter 1.6.2, A57G ELC mutation can cause functional changes in muscle fibers. Even though it is not as common as the mutations in MHC, it can cause malignant result such as SCD (Kazmierczak, Paulino et al. 2013). Because the A57 residual is located in the middle of the helix A in the EF- handed domain, the mutation of A57G can destabilize the helix (Serrano, Neira et al. 1992). Thus, the hypothesis is that A57G mutation in vELC will make the N-terminal extend more compared to the wildtype vELC. Since the pathomechanism of the A57G vELC mutation is still unknown, this study could provide some information to the puzzle. A chimera was designed for investigating the conformational effect of A57G ELC mutation by substituting endogenous rELC and rRLC on rabbit psoas fibers with exogenous A57G-vELC and vRLC in rabbit psoas muscle fiber. The conformational change of ELC due to the A57G-vELC mutation was studied directly by dynamic quenching measurement in vELC and vRLC reconstituted rabbit psoas skeletal muscle fiber in three states: rigor, relaxation, and contraction (Figure 12). Rat cardiac vELC was used as the background for studying the effect of A57G-vELC mutation. The amino acid similarity between human vELC and rat vELC is 96%, in which the amino acids flanking the A57G mutation show 100% similarity; the amino acid similarity between human vRLC and rat vRLC is 95%.

Cardiac labeled A57G-vELC was exchanged on the fiber. In order to measure the effect of ELC mutation on the conformation of myosin, the N-terminal C81 was labeled with IAEDANS. The acrylamide was used as the quencher to analyze the excitations and emissions of the fluorescent probes in the states of rigor, relaxation, and contraction of the muscle fiber. The ratio of amplitude-weighted average lifetimes τ_0 and

amplitude-weighted τ and the [Acrylamide] was linearly fit into the Stern-Volmer Equation and Stern-Volmer constant was compared for the WT (vELC•vRLC) and A57G (A57G-vELC•vRLC) (Figure 12). The different lifetimes, Stern-Volmer constants, quenching rate constants derived from the two quenching experiments, proved that the A57G mutation induced a conformational change of ELC, which made the C81 labeled site more exposed to the environment.

Chapter 2 Method

2.1 Expression and purification of ELC

Wildtype rat vELC were previously cloned into a pET3d expression vector (Novagen, Madison, WI), and the ELC with FHC mutation was created using the "QuikChange" Mutagenesis kit (Stratagene, CA). The ELC genes were transferred into an expression *Escherichia coli* cell line, BL21-AI. The cells were grown in luria broth (LB) media to log phase (OD_{600}=0.7 to 0.8) at 37℃ and then induced by 20% L-arabinose. The cells were grown for 3.5h after induction and centrifuged down at 6000rpm for six minutes.

2.2 Crude cell extraction and Ammonium Sulfate precipitation

The ELC was expressed in the cytoplasm, which was released from the cells using a lysis buffer (25mM Tris, pH7.5, 0.1M NaCl, 0.25M sucrose, 2mM EDTA, 2mM EGTA, .25mM DTT and 1mM PMSF). The cell membrane was further broken by the sonicator to release the protein in the cells to the buffer. The high molecular weight protein was precipitated with 45% solid ammonium sulfate (SAS) after the addition of 5M urea. Then low molecular weight proteins including ELC were precipitated with 80% SAS.

2.3 Further purification with column chromatography

To further purify the ELC, the protein was loaded onto an anion exchanger DEAE FF and purified in column (TRIS) buffer (25mM Tris-HCl, pH7.5, 0.2mM EDTA, 0.1mM DTT) with a NaCl linear gradient (50mM to 300mM). Previously, a higher final NaCl concentration of 500mM was performed for the linear gradient and another gel filtration column was used with 5M urea. In some cases, the final product was shown

as either not pure enough or denatured by SDS PAGE analysis. After purification, the gradient fractions were analyzed and pooled together and then dialyzed six times against 4 liters of 25mM ammonium bicarbonate buffer with 0.1mM DTT in it for lyophilization. The lyophilized ELC was stored at -20 ℃ until needed. The lyophilized ELC was exchanged into muscle fibers as described by Roopnarine et al (Roopnarine, Szent-Györgyi et al. 1998).

2.4 Expression and purification of RLC

Wildtype rat vRLC were previously cloned into a pET3d expression vector (Novagen, Madison, WI), and the ELC with FHC mutation was created using the "QuikChange" Mutagenesis kit (Stratagene, CA). The vRLC genes were transferred into an expression cell *Escherichia coli* cell line, BL21-AI. The cells were grown in luria broth (LB) media to log phase (OD_{600}=0.7 to 0.8) at 37 ℃ and then induced by 20% L-arabinose. The cells were grown for 3h after induction and centrifuged down at 6000rpm for six minutes.

The RLC was expressed in inclusion bodies, and the cells were broken with lysis buffer (25mM Tris, pH 8.5, 5mM EDTA, 50mM glucose, 1mM PMSF, 1mM DTT, 0.15mg/ml lysozyme), followed by a freeze/thaw cycle. The mixture was incubated with 10mM $MgCl_2$ and 25 ug/ml DNase I for one hour on ice. The inclusion bodies were centrifuged down at 11,500 rpm at 4 ℃ and first washed in the lysis buffer +0.1% triton ×100 twice, then in triton-free lysis buffer. The RLC was purified from the inclusion bodies by adding column buffer (50mM MOPS, pH6.5, 10mM NaCl, 1mM DTT) with 7M urea in it, and loaded on a DE52 anion exchange column. A linear NaCl salt gradient in 4M urea column buffer was performed. The purity of gradient fractions was visualized by 12% SDS PAGE and only the pure fractions were pooled and dialyzed against 4L (130Kpr, 25mM MOPS, 2mM $MgCl_2$, 1mM EGTA, 1mM NaN_3)

and 0.1mM DTT six times. The RLC was concentrated to about 6mg/ml and stored in liquid Nitrogen until needed.

The rabbit skeletal troponin C (TnC) was extracted from the rabbit muscle ester powder, as described previously (Potter 1982). Protein concentrations were determined by the Biorad assay, using bovine serum albumin as the standard.

2.5 ELC labeling with IAEDANS

The purified wild type and mutant ELC were labeled with the fluorescent probe IAEDANS at C81 (Figure 13) for quenching measurement. The ELC were reduced by 6M Guanidine HCl reducing solution (6M Guanidine HCl, 10mM MOPS) for 30 minutes at room temperature and final concentration (about 6mg/ml) and then dialyzed against 4 L NaPO buffer (5mM sodium phosphate [monobasic and dibasic], pH 6.5, 50mM NaCl, 1mM $MgCl_2$ and 1mM NaN_3) three times. The pH of the protein solution was increased from 6.5 to 8 after dialysis. The protein concentration was determined by Biorad assay and micromoles of the protein were calculated using Equation 1.

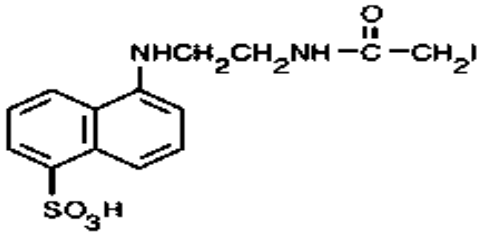

Figure 13. Structure of 1,5- IAEDANS.

$$Micromoles = \frac{[Protein]mg/ml}{20{,}700} \times 1e^{6} \quad \textbf{(1)}$$

The amount of IAEDANS added was five-fold of the micromoles of protein. The concentration of IAEDANS was determined using the absorbance and extinction coefficient of [dye] =absorbance$_{336nm}$*dilution factor, and the micromoles of the IAEDANS was calculated by Equation 2.

$$Micromoles = \frac{[IAEDANS]mg/ml}{5700} \times 1e^{6} \quad (2)$$

The volume of IAEDANS needed was calculated using the volume of the protein and the micromoles of the protein to be labeled and micromoles of the IAEDANS by Equation **(**3. It was stirred overnight with reduced ELC at 4 ℃.

$$Volume\ of\ IAEDANS = \frac{Volume\ of\ protein\ sample \times 5 \times micromoles\ of\ protein\ sample}{Micromoles\ of\ IAEDANS} \quad (3)$$

The excess dye was removed by using zeba spin columns, and the dye-to-protein ratio was calculated from the ratio of the micromoles of dye (Equation 2) to the micromoles of the protein in the labeled sample (Equation1). Characterization of successful labeling and removal of free dye were done by 15% SDS PAGE. The fluorescent bands were observed under UV light.

2.6 Preparation of muscle fibers

Rabbit psoas fibers were prepared as described previously (Roopnarine 2003). The fiber bundles were about 0.4cm in diameter and incubated in fiber storage solution (FSB=50%v/v Rigor solution(RS)/glycerol solution (RB:130mM potassium propionate, 2mM $MgCl_2$, 1mM EGTA and 20mM MOPS, pH7.0), 1uM pepstatin, 1uM leupeptin) for 1 hour at 4 ℃ three times, and then stored at -20 ℃ for six weeks for full permeabilization.

2.7 Extraction of native rELC, rRLC and reconstitution with wildtype ELC and mutant ELC, vRLC and rRLC for different chimeras, respectively.

The fibers were dissected into thinner bundles (~0.4-0.5mm in diameter); the ends were tied with silk thread and placed in the glass capillaries. The capillaries were attached to a peristaltic pump for extraction of RLC and ELC and the speed was

controlled at 0.5ml/min. For RLC extraction, the fiber bundles were washed with extraction buffer (20mM Imidazone, pH7.0, 20mM KCl, 10mM EDTA, 10mM CDTA, 2mM EGTA, for 10 minutes at 4 ℃) as described previous (Roopnarine 2003) and then washed with RLC extraction buffer (extraction buffer containing 10mM DTNB for 25 minutes at room temperature). The fibers were then washed by extraction buffer for 7 minutes at 4 ℃. To extract ELC, the fiber bundles were washed by extraction buffer with 1.5mM TFP for 3 hours at 4 ℃, and then washed with RB, pH 7 that was followed by RB, pH8. To remove 5-thio-2-nitrobenzoic acid-modified cysteine, the fiber bundles were then incubated in RB (pH 8) with 30mM DTT for 4.5h at 4 ℃ and then washed by RB (pH 7) for 10 minutes to remove all DTT. For Tn complex reconstitution, the Tn complex solution (20mg/ml) was added to the fiber bundles in RB (pH 7) plus 10mM Mg-ATP and incubated for 2 hours at 4 ℃, the TnC solution was removed after incubation and the fiber bundles were washed with RB (pH 7). For either wildtype or mutant ELC reconstitution, the fiber bundles were immersed in each type of ELC solution respectively for 2 hours at 4 ℃. The ELC solution was removed and fibers were washed with RB (pH7).

To reconstitute vRLC and rRLC, the fibers were incubated in RLC solution for 2 hours and then washed by RB (pH7). The fiber bundles were washed by FSB solution and stored in FSB containing 1uM pepstatin and 1uM leupeptin. The extent of ELC and

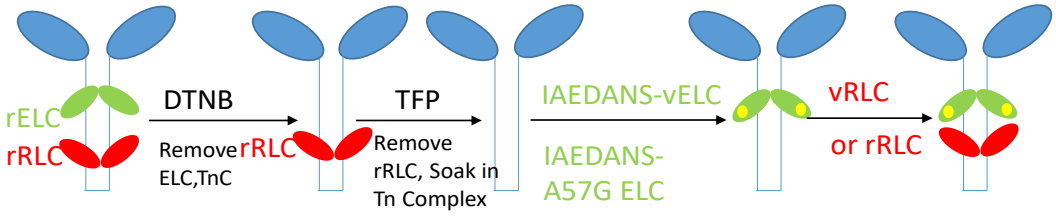

Figure 14. The extraction of TnC, rELC and rRLC on fibers and reconstitution with TnC, vELC or A57G-vELC, vRLC or rRLC. To reconstitute fibers with IAEDANS-vELC, TnC and rRLC need to be removed first. The fibers are then reconstituted with TnC, IAEDANS-ELC and then vRLC or rRLC.

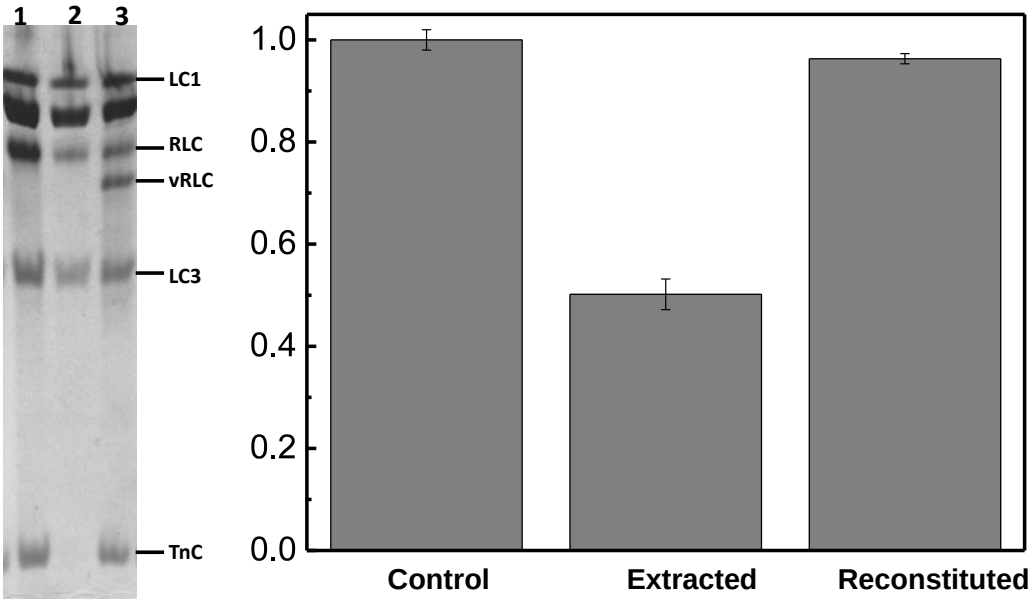

Figure 15. The ELC and RLC extraction and reconstitution (Roopnarine and Price 2014)
Left: the 15% polyacrylamide urea gel of muscle fiber proteins; lane 1 is the control muscle fibers; lane 2 is the ELC and RLC extracted muscle; lane 3 is the reconstituted fibers

RLC reconstitution was determined by densitometry analysis of 15% polyacrylamide urea (Tris-borate) gels (Biorad, Richmond, CA).

The native ELC and RLC were extracted using previously documented protocol (Roopnarine and Price 2014). Here it was shown that the previous results of the extraction procedure removed ~50% LC1+ LC3 and RLC, and 100% TnC (Figure 17). and the reconstruction of vELC and vRLC was achieved with the mechanical properties of the fibers were restored (Figure 15).

2.8 Rigor, relaxation, and contraction Solutions

The solutions used for the fiber experiment during fluorescence quenching were as described previously (Roopnarine, 1995). The rigor solution was 190mM potassium propionate (Kpr), 2mM $MgCl_2$, 1mM EGTA, and 20mM MOPS (pH 7). The relaxation

solution was 20mM Kpr, 2mM MgCl2, 1mM EGTA, 20mM MOPS, 5mM Mg-ATP, 50mM creatine phosphate, 750 units/ml creatine kinase (CK) (pH 7). The EGTA-rigor solution was 10mM EGTA + rigor solution. The contraction solution was relaxation solution plus 1.5mM $CaCl_2$ (pH 7).

2.9 Time-resolved fluorescence quenching

2.9.1 Instrument set up

All time-resolved fluorescence waveforms were acquired using high performance fluorometer that constructed in the Biophysical Technology center, University of Minnesota (Figure 16). This instrument uses direct waveform recording, which allowed the recording of the data with comparable signal/noise, accuracy and resolution of distinct component with time-correlated single-photon counting. The samples were excited by a passively Q-switched microchip YAG laser pulse (model NanoUV-532; JDS Uniphase) at 355 nm with a pulse repetition frequency of 10 kHz. The pulse energy is 1μJ/pulse and the pulse width is about 1 ns. The intensity and shape of the laser pulses are highly uniform. The emitted fluorescence was filtered by an 470/20 nm interference band-pass filter and then collected with a photomultiplier tube module (H5773-20, Hamamatsu), and digitizer (Acqiris DC252; time resolution, 0.125 ns).

2.9.2 Experimental design

The instrument response function (IRF) was recorded using water. The dynamic quenching experiments were performed at 22 ℃. The fluorescence waveforms were acquired in rigor, relaxation and contraction solutions for each type of the chimera. The IAEDANS probe was excited at 355 nm and the emission decays were acquired at 470nm ±20 nm. The labeled muscle fibers were tied carefully with fine forceps vertically to a holder, then placed in a cuvette and stored in FSB until needed (Figure

16, upper left). The fibers were cut into be approximately 1cm in length. The quenching solution was made from rigor, relaxation, and contraction buffer with 6M acrylamide solution. The [acrylamide] was 0M, 0.075M, 0.1M, 0.150M, 0.2M, 0.3M, 0.4M, and 0.5M respectively.

2.9.3 Data analysis

The observed waveform was fitted by a simulation $F_{sim}(t)$, consisting of a multi-exponential decay F(t) convoluted with the IRF.

$$F(t) = \sum_{i=1}^{n} A_i \exp\left(\frac{t}{\tau_i}\right) \quad \textbf{(4)}$$

$$F_{sim}(t) = \int_{-\infty}^{+\infty} IRF(t - t')F(t')dt'$$

where τ_i is the fluorescence lifetime of the *i*th component. The difference between the theoretical curve and the data was evaluated from the plot of residuals and the reduced Chi-square (χ^2) .

The waveforms were analyzed using the Stern-Volmer equation

$$\frac{\tau_0}{\tau} = 1 + K_{sv}[Q] \quad \textbf{(5)}$$

$$K_{sv}=k_q\tau_0 \quad \textbf{(6)}$$

in which τ_0 and τ are the amplitude-weighted lifetimes for WT-ELC and FHC-ELC, respectively. The amplitude-weighted lifetime is defined as $\tau_{ave}=\Sigma a_i\tau_i/\Sigma a_i$. The amplitude-weighted lifetimes are the better type of "average" lifetime to use in dynamic quenching because the amplitude average lifetime leads to linear Stern-Volmer plot at low quencher concentrations and the bimolecular quenching constant (k_q) reflects

closely the k_q of the major component in dynamic quenching. (Sillen and Engelborghs 1998). In Equation 5, [Q] is the molar concentration of the quencher, acrylamide, and Ksv is the slope or Stern Volmer constant for quenching (Szymanski, Jezewska et al. 2013). The slope, K_{sv}, was determined for each sample by plotting the τ_0/τ vs [Acrylamide]. The

2.10 Statistical Analysis

The one-way analysis of variance (ANOVA) was used to determine the significance of the difference between the means of three groups and the one-tailed paired Student's *t* test analysis was used to assess the significance of two groups by Origin (Origin Lab, Northampton, MA).

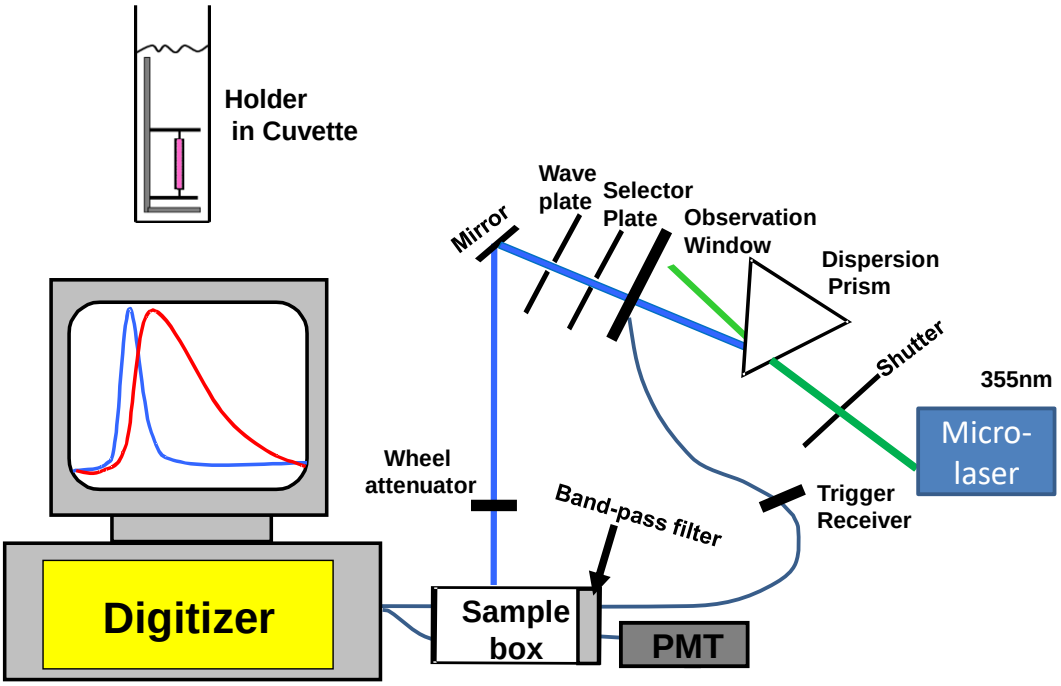

Figure 16. Experimental setup. The isolated permeabilized muscle fibers were tied isometrically in the two pins on a holder and then put in a cuvette with solutions. The experiment was controlled at 22 ℃. A 470 ±20nm band-pass filter was used. The shutter, dispersion prism, and observation window were aligned to allow light to pass through. The 355nm wavelength was selected by the selector plate and changed to linearly polarized light by wave plate. The bottom of the mirror needed to be aligned with the center of the hole in the sample box so that the light with 355nm wavelength could hit the sample. The sample was then the isometrically tied permibilized muscle fiber in the cuvette (upper left of the figure).

Chapter3 Results

3.1 ELC purification with unmodified procedure

The ELC-containing solution was loaded onto an ion-exchange column that was eluted with gradient starting at 50mM NaCl and ending at 500mM NaCl at 5ml/min. The ELC containing fractions eluted soon the gradient elution started as shown in Figure 17. The first peak corresponded to the ELC and second peak corresponded to the high molecular weight impurities that bind to the column tighter and eluted with higher ionic strength. This indicates that ELC was completed eluted when the [NaCl] reached about 150mM and the ionic strength was not very high. The result from the next step of gel filtration was shown in Figure 17 A. The high molecular impurities were not removed, and some denatured products were detected by SDS PAGE. The loading protein from crude extraction was 53mg and the yield include impurities was 17mg so the percent yield was 32%.

3.2 ELC purification after modification

Instead of ending with 500mM NaCl, the elution gradient ended with 300mM, which was a lower ionic strength. The crude extraction procedures remained the same. In Figure 18, the impurities were not eluted along with ELC when the ionic strength was low, and there was no sign of protein denaturation at the low molecular weight section of the gel. The initial loading total protein weight was calculated by multiplying the concentration of the crude extracted solution by the total volume. The percent yield of ELC was the ratio of the final pure ELC weight, which was 37.13mg, and the initial loading weight, which was 52.5mg. The ELC percent yield was increased from 32% to 71%.

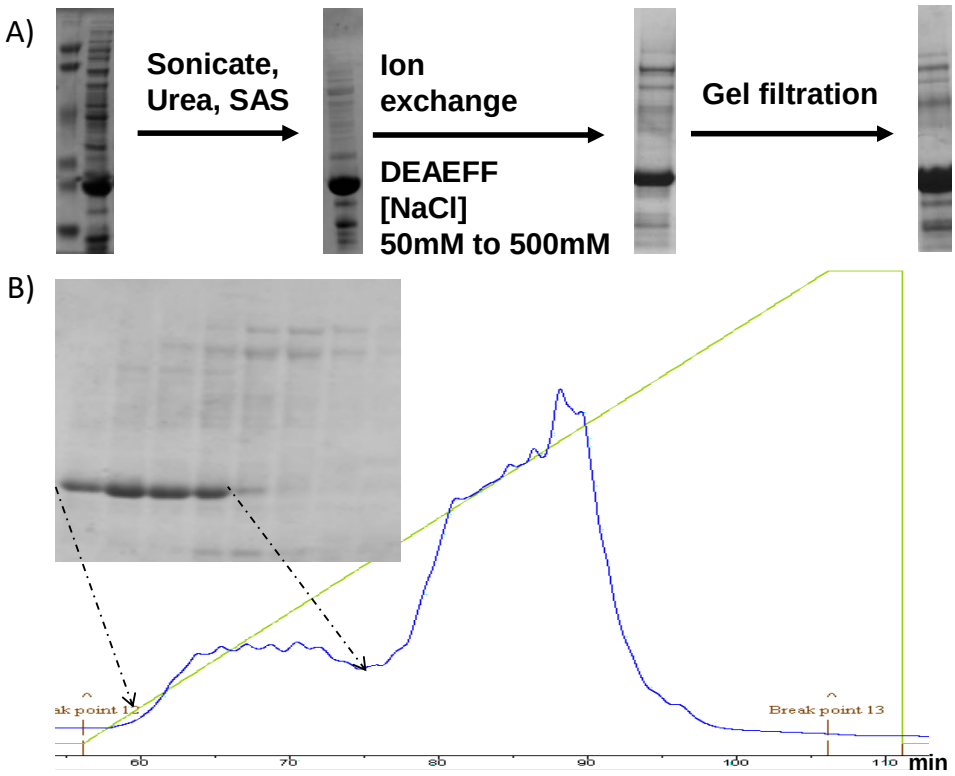

Figure 17. A). SDS PAGE profile assessment of previous ELC purification procedure. 15% Tris-HCl SDS PAGE gel lanes showing purification of ELC from E. coli cells with different procedures including sonication, Urea, and ammonium sulfate precipitation. B) The 15% Tris-HCl SDS PAGE gel lanes showing the pool fraction and the absorbance corresponding to the gradient elution. There are two peaks from the gradient elution, however, only the first peak contains ELC and the other fractions contain high molecular weight impurities.

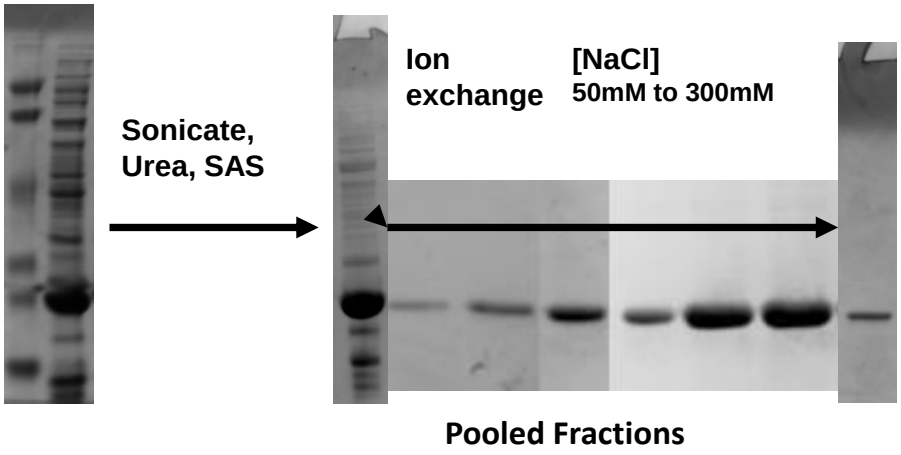

Figure 18. SDS PAGE profile from improved purification procedure.
The 15% Tris-HCl SDS PAGE gel lanes showing purification of ELC from E. coli cells from the modified elution gradient: 50mM to 300mM elution.

3.3 C81-ELC Labeling

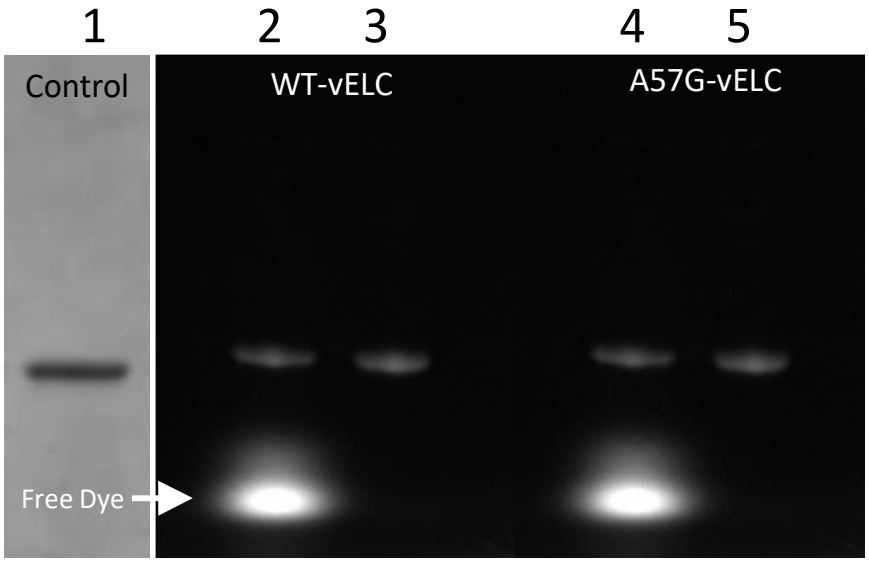

Figure 19. SDS-PAGE profile under ultraviolet light. The first lane is the ELC control, the second lane is WT-ELC before removing the free IAEDANS label. The third lane is WT-vELC after removing the free IAEDANS dye. The 4th lane is A57G-vELC labeling followed by FHC-ELC after removal of the free dye.

The IAEDANS labeling results for both WT-vELC and A57G-vELC were subjected to the 15 % SDS-PAGE (Figure 20). The first lane was the ELC control that stained by Coomassie Blue and the ELC band was at about 20kD. The IAEDANS

labeling was successful for both WT- and A57G-vELC with fluorescent bands showed up at the 20kD which is the vELC band position. The second and third lanes contain IAEDANS-WT-ELC. The free dye was not shown at bottom of third lane and this showed that free dyes were successfully removed by zeba column and showed in the third lane. IAEDANS-FHC-ELCs were in the last two lanes. Free dye in lane 4 was all managed to be removed and thus no free dye in lane 5. The calculated dye to protein ratios for the labeling of the WT-vELC and A57G-vELC were 0.90 and 0.92, respectively. Thus, the IAEDANS labeling of C81 was efficient.

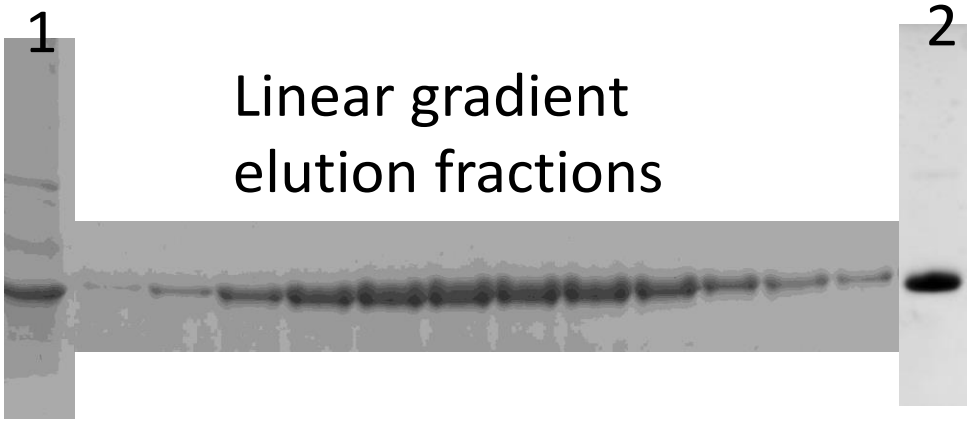

Figure 20. SDS-PAGE profile of RLC purification before and after DE52 anion exchange column. Lane 1 is the SDS-PAGE profile before loading onto anion exchanger. The following lanes are for the fractions that correspond to linear gradient elution. Lane 2 is the profile for RLC purification lyophilized product.

3.4 RLC purification

The RLC purification was characterized by SDS PAGE (Figure 20). After raw RLC extraction from cell inclusion bodies, the RLC containing solution was loaded onto a DE52 anion exchanger. The gradient fractions were analyzed by 15% SDS PAGE. As shown in Figure 20, the fractions already contained pure RLC; the purity was further proved by the SDS PAGE profile of RLC lyophilized powder in lane 2.

3.5 Multi-exponential fits

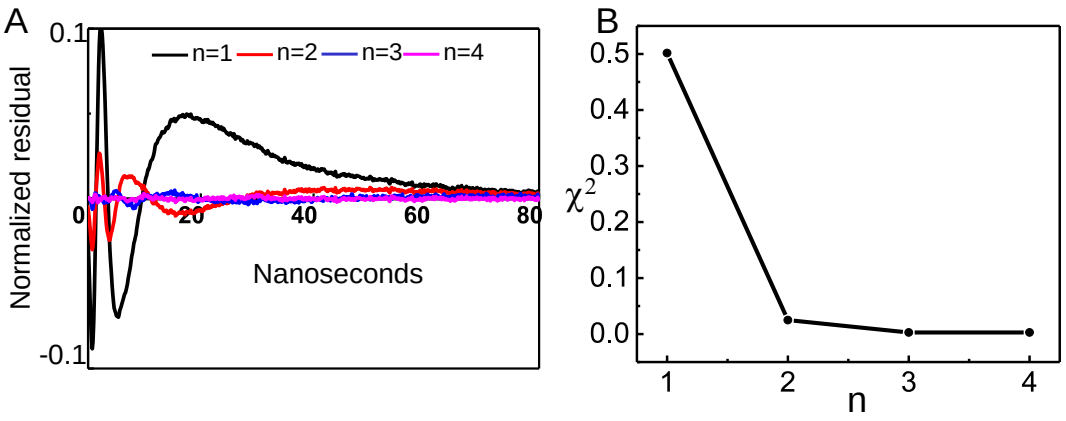

Figure 21. Time-resolved fit of WT, in rigor (0 M acrylamide) A) Normalized residuals (experimental data-data fit/maximum fit value), for fits with equation 4 for n=1-4, B) reduced χ^2 values, 0.502, 0.025, 0.003, 0.003 for n=1-4.

The fluorescence of the all samples was fitted by Equation 4, varying the number of exponentials (n) from 1 to 4. In all cases, residuals and χ^2 values were improved by increasing n to 3, but there was no further improvement for n=4, as shown for the vELC and vRLC wildtype (WT) reconstituted fiber in rigor without acrylamide in Figure.

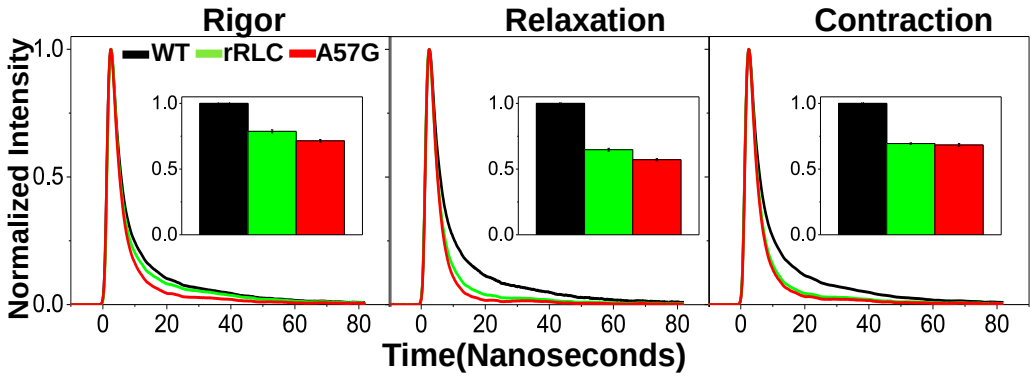

Figure 22. Fluorescence waveforms of IAEDANS-labeled vELC and vRLC (WT,black) and rRLC (green) reconstituted muscle fibers, and fluorescence life time of IAEDANS labeled A57G-vELC(A57G, red) reconstituted muscle fibers for rigor, relaxation, and contraction states. The normalized amplitude weighted τ_0 of WT, rRLC and A62G in rigor were plotted in the bar chart. For rigor, the τ_0 were 2.37±0.053ns, 1.94±0.002ns, 1.70±0.022ns, respectively for WT, rRLC and A57G before normalized with rigor τ_0. For relaxation, the τ_0 were 2.72±0.01ns, 1.76±0.02ns, and 1.55±0.015ns for WT, rRLC and A57G, respectively, before normalized with relaxation τ_0. For contraction, the τ_0 were 2.68±0.01ns, 1.86±0.01ns, and 1.85±0.022ns for WT, rRLC and A57G before normalized with contraction τ_0. n=2, respectively.

3.6 The Fluorescence lifetime in the absence of the quencher of reconstituted permeabilized muscle fibers

To assess the structural effect of different RLC sources on ELC and A57G-vELC mutation, the C81 sites for vELC and A57G-vELC were labeled with fluorescent probe, IAEDANS. The τ_0 is defined as the lifetime in the absence of the quencher. As shown in Figure 22, the WT (black) is vELC and vRLC chimera. The τ_0 was compared with the rRLC (vELC-rRLC, green) and the A57G (A57G-vELC-vRLC, red). Both rRLC and A57G had shorter τ_0 for states of rigor, relaxation, and contraction. The fluorescent probe was also sensitive to the microenvironment so that the degree of lifetime decay was different in these three states. The A57G had the shortest τ_0, thus, compared to the rRLC, the presence of A57G-vELC mutation perturbed the microenvironment of the probe more.

When the fibers were placed in different solutions, for all chimeras, the rigor solution resulted in the highest τ_0 and the relaxed fibers had the lowest τ_0 (Figure 23). The τ_0 in the WT was not significant in rigor, relaxation, and contraction states, but the difference became significant for the rRLC and A57G. Thus, there was a small structural change of vELC conformation for WT and the changes became significantly larger in the rRLC and A57G when soaking the fibers in rigor, relaxation, and contraction solutions. The conformational shift was consistent across different chimeras but became larger for the rRLC and A57G-vELC reconstituted fibers.

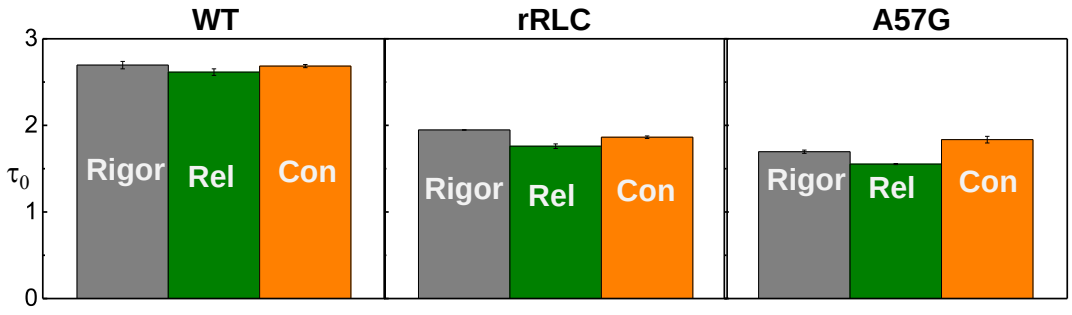

Figure 23. Bar chart for τ_0 comparing rigor, relaxation and contraction
The lifetimes in the absence of the quencher (τ_0) was plotted with rigor (▪), relaxation (•), and contraction (▪) conditions as x axil for WT, rRLC and A57, three chimeras. For all three chimeras, the rigor contained the highest τ_0 and the relaxation contained the lowest τ_0, except for WT where the difference was not significant. The contraction gave an intermediate τ_0.

3.7 The fluorescence lifetime decreased with increased [acrylamide]

Fluorescence lifetime was used to monitor quenching of the probe by acrylamide. Static and dynamic quenching can be distinguished by lifetime measurement. (Lakowicz 2006). Furthermore, monitoring lifetimes made it easier to exclude static quenching artifacts (Eftink and Shastry 1997). Because static quenching can also result in linear Stern-Volmer plot, it is important to make sure the lifetime τ decreases when the concentration of the quencher is increasing. In Figure 24, the fluorescence waveforms were shown with gradient color for the WT, rRLC and A57G for rigor state and the average lifetimes for these three chimeras were plotted with [acrylamide] increasing from 0 to 0.5 M. The lifetimes were all decreased as quencher concentration increased. Thus, the quenching was confirmed to be dynamic and the ratio of τ_0 and τ could be used for the Stern-Volmer plot.

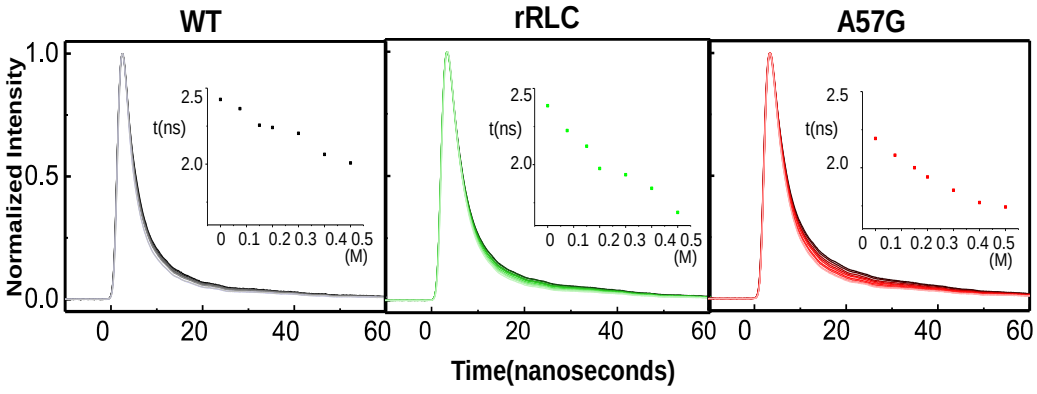

Figure 24. Fluorescence lifetime waveforms showed quenching decay for WT (black), rRLC (green) and A57G (red) in rigor. The inset scatter plot was the decreasing τ vs. [acrylamide].

3.8 Stern-Volmer plots for rigor, relaxation and contraction of WT, rRLC and A57G

In Figure 25, all Stern-Volmer plots were shown with the color-coded corresponding Stern-Volmer constants (Ksv) in the table; the rRLC and the A57G were compared with the WT in rigor, relaxation, and contraction. The Ksv values for the WT were the lowest in all states: rigor (0.40 ±0.04 M^{-1}), relaxation (0.41 ±0.01 M^{-1}), and

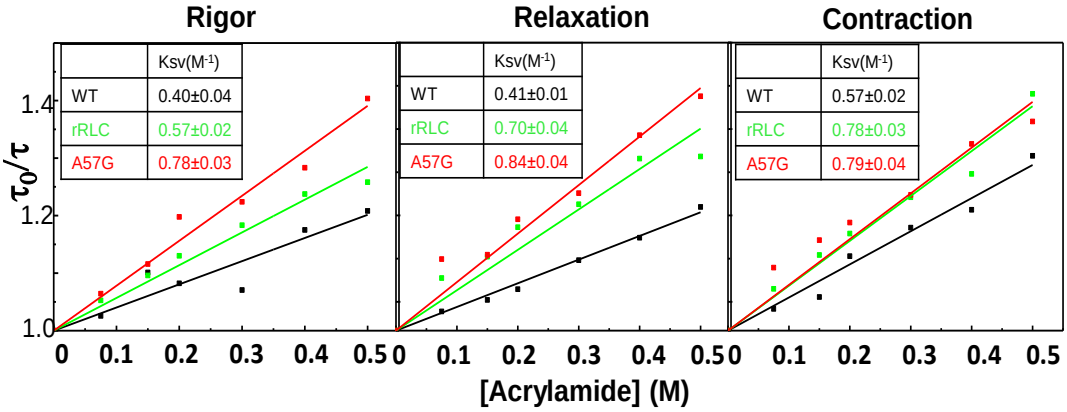

Figure 25. Stern-Volmer quenching plots for WT (black), rRLC (green) and A57G (red) in rigor, relaxation, and contraction. The concentration of quencher was increased from 0 to 0.5M. In rigor, Ksv was 0.40 ±0.04 M^{-1}, 0.57 ±0.04 M^{-1}, and 0.78 ±0.03 M^{-1} for WT (•), rRLC (•), and A57G (•), respectively. In relaxation, 0.41 ±0.01 M^{-1}, 0.70 ±0.04 M^{-1}, and 0.84 ±0.04 M^{-1} for WT (•), rRLC (•), and A57G (•), respectively. In contraction, 0.57 ±0.02 M^{-1}, 0.78 ±0.03 M^{-1}, and 0.79 ±0.04 M^{-1} for WT(•), rRLC(•), and A57G(•), respectively.

contraction (0.57 ±0.02 M^{-1}) (Figure 25). The rRLC quenching data gave higher Ksv values for all states but not as high as the Ksv for the A57G. The acrylamide was effective in both rRLC and A57G. Stern-Volmer quenching plots of the comparison between the rRLC and WT in three panels indicated that different RLC isoforms would affect the ELC conformation. The effectiveness was stronger in the A57G for rigor and relaxation, thus the presence of A57G mutation in ELC affected the ELC conformation more, compared to the perturbation of RLC isoforms in rigor and relaxation. The perturbation in the contraction state was comparable for ELC mutation and different RLC isoforms.

3.9 Transition from pre-powerstroke to powerstroke

Table 1. Transition from pre-powerstroke to powerstroke. Transition from pre-powerstroke to powerstroke= Ksv contraction/Ksv relaxation

	Ratio
WT	1.39 ±0.12
rRLC	1.11 ±0.09
A57G	0.98 ±0.11

The transition from pre-powerstroke to powerstroke is defined as the ratio between the Ksv contraction and the Ksv relaxation (Table 1). The smaller the ratio, the less conformational change exists due to powerstroke performance; if the ratio is closed to one, the conformational change is not noticable. In Table 1, the conformational change due to contraction in the WT is larger than that in the rRLC. In addition to that, there is not much conformational change in the A57G from pre-powerstroke to powerstroke.

3.10 Bimolecular Quenching Constants

The bimolecular quenching constants for time-resolved quenching of three chimeras in rigor, relaxation, and contraction were calculated from the quenching constants determined in Stern-Volmer plots according to Equation **(**5) (Table 2). The k_q reflects the accessibility of the fluorophores to the quencher and the efficiency of the quenching (Lakowicz 2006). In all three states (rigor, relaxation, and contraction), the fluorescent probe in the WT was least accessible compared to the probe in the rRLC and the A57G reconstitution fibers. To compare more conveniently, the ratio of k_q for the rRLC and the A57G with WT was calculated (**Error! Reference source not found.**, last column) in rigor, relaxation, and contraction, respectively. The rRLC probe's accessibility to the quencher was different from that in WT for rigor, relaxation, and contraction. The probe in the A57G contained the most accessibility to the quencher in

the solvent for three states. To assess the response of the probe to the rigor, relaxation, and contraction conditions, the k_q was plotted for each chimera with three categories in each panel (**Error! Reference source not found.**). The k_q was always the highest in the relaxation and lowest in rigor for the three different chimeras.

Table 2. Biomolecular Collision (k_q) for WT, rRLC and A57G in rigor, relaxation and contraction. The errors were calculated by propagation of Ksv errors. Ratio was calculated from k_q of rRLC and A57G to WT in rigor, relaxation and contraction.

		$k_q \times 10^8$ ($M^{-1}s^{-1}$)	Normalized to WT
Rigor	WT	1.49 ±0.16	1.00
	rRLC	2.92 ±0.184	1.96
	A57G	4.60 ±0.17	3.08
Relaxation	WT	1.57 ±0.06	1.00
	rRLC	3.98 ±0.21	2.52
	A57G	5.42 ±0.20	3.44
Contraction	WT	2.14 ±0.07	1.00
	rRLC	4.18 ±0.08	1.95
	A57G	4.32 ±0.18	2.02

Chapter 4 Discussion

4.1 Protein purification from modified procedure and ELC, RLC reconstitution

The modified procedure utilized a less steep gradient of 0-500mM NaCl, which was successful in separating the ELC from the contaminating bacterial proteins a s shown in the SDS-PAGE profile in the gradient fractions and the final lyophilized product (Figure 18). The yield was also increased by 100%, which is likely due to less protein loss when using one type of chromatography rather than two.

The ELC labeling was successful with extra dye removed and the labeling efficiency was high. Although the direct quantification of the reconstituted fibers were not done, the high signal/noise in the time-resolved fluorescence quenching measurements could confirm the success and efficiency in labeled vELC reconstitution. In addition, the protocols used in the exchange and reconstitution of ELC and RLC were previously documented which achieved 60% ELC and 50% of RLC reconstitution and restored the mechanical properties of the fibers (Roopnarine and Price 2014) (Figure 15). Previously reported work showed that the ability of reconstituted muscle fiber to activate following ELC and RLC exchange was largely preserved (Roopnarine 2003; Knowles, Ferguson et al. 2008; Ushakov, Caorsi et al. 2011). The ELC and RLC bound to the IQ1 and IQ2 sequence, respectively, with high specificity. The unoccupied IQ1 and IQ2 sequence can bind the ELC and RLC, respectively, from virtually any species presented to it *in vitro* (Wagner and Weeds 1977; Sellers, Chantler et al. 1980; Ushakov, Caorsi et al. 2011). The exchange of native ELC and RLC with mutated protein or variants allows the creation of different hybrids for investigation of conformational or functional change of muscle fibers *in vitro* due to different substituted proteins.

4.2 Fluorescence quenching measurements

The fluorescence quenching technique was applied to probe the interactions between ELC and RLC as well as the A57G-induced ELC conformational change. The waveforms were fitted into three exponential decays, which gave the smallest χ^2 and residuals (Figure).The decreasing of fluorescence lifetimes corresponding to the increasing concentration of the quencher (Figure 24) and the linear Stern-Volmer plots (Figure 25) proved that dynamic quenching occured and only one type of fluorophore exists since no curvature was observed in the fits. A theoretical calculated efficient quencher k_q for a free fluorophore should be about 7×10^9 $M^{-1}s^{-1}$, and the k_q value can be reduced for biomacromolecular assemblies due to steric or electrostatic factors (Dewey 1991). The acrylamide quenching of Trp residues in globular proteins can range from 1×10^7 to 1×10^9 $M^{-1}s^{-1}$ (Eftink 2000). The k_q values derived in the present work were ranged from 1.49×10^8 $M^{-1}s^{-1}$ to 5.42×10^8 $M^{-1}s^{-1}$ (**Error! Reference source not found.**), which were reasonable in biomacromolecular assemblies. The time-resolved fluorescence quenching studies can provide structural information concerning the exposure of fluorophores in proteins (Hennecke, Sillen et al. 1997). By focusing one specific site, the information about the microenvironment of the probe should be provided (Hennecke, Sillen et al. 1997).

4.2.1 Conformational change in vELC due to skeletal rRLC

The fluorescence lifetimes in the absence of the quencher was τ_0. In this study, the τ_0 of the WT was the longest in all solutions (rigor, relaxation and contraction) compared to the other two chimeras, the rRLC and the A57G (Figure 22 and Figure 23). It is suggested that the probe at C81 in vELC might be more buried and less

exposed to the solvent for the WT. This is consistent with the previous works for scallop and vertebrate smooth muscle that the ELC N-lobe is in the closed conformation (Houdusse and Cohen 1996; Dominguez, Freyzon et al. 1998).

The τ_0 for the rRLC was shorter than the WT in all conditions (Figure 23 and Figure 24). This demonstrated that the C81 probe was more exposed to the solvent compared to the WT. Since the fluorescence lifetime tend to be shorter in more polar environments (Munishkina and Fink 2007), the N-terminal of ELC is in a more open conformation in the rRLC and A57G compared to the WT. This is also consistent with the Ksv values. Compared to the Ksv values derived from WT, the rRLC contains a higher Ksv for all rigor, relaxation, and contraction (Figure 25). The conformational change of vELC which is more open in the rRLC was due to the existence of skeletal rRLC, this indicated that specific isoform of RLC is required for in muscle fiber contraction and the interaction between vELC and vRLC existed in the WT. From the crystal structure of myosin S1 (Figure 4), the N-terminal of ELC and C-terminal of RLC are at a reasonable distance to interact to form a salt bridge. Previous studies in scallop myosin also demonstrated that the contact area involved between ELC and RLC is limited but important when F20 and R24 residuals of the ELC form hydrogen bonds with G117 of the RLC and these bonds allow close contact between the G23 of the ELC and G117 of the RLC (Xie, Harrison et al. 1994).

The ratio between Ksv contraction and Ksv relaxation was smaller in rRLC, which indicates, that the powerstroke do not cause as much structural change in rRLC as compared to WT. Because powerstroke generate force, when use WT as a basis, the existence of skeletal RLC can affect force generation. Previous works have shown that the interactions between RLC and ELC have regulatory importance for activation of smooth muscle (Ni, Hong et al. 2012; Taylor, Feig et al. 2014).

4.2.2 Conformational change in vELC due to A57G mutation

The A57G mutation was discovered in two Korean families and one Japanese patient with hypertrophic cardiomyopathy (Lee, Hwang et al. 2001). The present study was focusing on the conformational changes in the vELC induced by the A57G-vELC mutation in rigor, relaxation and contraction states. .

The τ_0 for the A57G were shorter than the WT in all conditions (Figure 23 and Figure 24). In addition to that, the Ksv values for the A57G in all three conditions are higher than that in the WT. Both of these facts demonstrate that the C81 probe is waore exposed to the solvent in the A57G than compared to the WT. Since the Ksv values are higher and the τ_0 for the A57G are lower than those of the rRLC, the A57G mutation induced the vELC to extend more compared to the existence of skeletal rRLC. The less shielded C81 labeled sites indicate that the A57G-vELC in the reconstituted experimental fibers is less immobilized and more flexible. The data was comparable to the previously reported works that A57G-vELC bound slightly but significantly weaker to the myosin IQ1 site (Lossie, Ushakov et al. 2012). The data also correspond to the fact that an unstable structure can be induced by Ala to Gly in the helix mutation (Serrano, Neira et al. 1992) since the A57G is in the helix A of the first EF-handed domain (Figure 8 and Figure).

When comparing the Ksv values in rigor, relaxation and contraction for the A57G-vELC, its Ksv values are not changing as much as the Ksv values for the WT are. The Ksv values are also remained to be high in these three conditions. These facts indicate that the A57G mutation make the vELC structure be loose or extended constantly and that the Mg-ATP and actin-binding do not induce as much vELC conformational

change as the vELC in the WT. Therefore, the helix A, which is the location of the A57G cardiomyopathy mutation, can be disrupted or destabilized due to the mutation. This is also consistent to the result of previous work which showed that A to G mutation in helix can make the structure unstable (Serrano, Neira et al.1992). Thus, it is reasonable to conclude that the activation of myosin that was required for cardiac contraction was disturbed due to the ELC mutation, and the A57G mutation could exert its effect through a cross-bridge-myosin backbone interaction. This was consistent with the previous studies which showed that A57G decreased maximal force generation (Kazmierczak, Paulino et al. 2013) and one possible disease-causing mechanism was the disruption of N-ELC and actin interactions (Muthu, Wang et al. 2011).

4.3 Conclusion

The dynamic quenching measurement is a useful technique to investigate conformational changes of proteins. The acrylamide is a strong quencher. There is an ELC and RLC interaction, which is probably essentially important for cardiac contraction. The potential salt-bridge bets are between K63 (vELC), and E120 (vRLC), D60 (vELC) and K114 (vRLC) and K55 (vELC) and D116 (vRLC). The amino acid sequences (SLKADYVR) of the vRLC before the E120 area are complete different from those (TIKKQFLE) of the rRLC; the unaligned sequences belong to the linker area in the RLC 3rd EF-hand domain (Figure). The unaligned sequences in vRLC and rRLC form the linker area in the third EF-handed domain, which is in closed contact between ELC and RLC (Xie, Harrison et al. 1994). The unalignment can break the last two listed salt bridges and this may account for the more open local ELC structure of vELC when the skeletal RLC isoform present. The A57G mutation causes the helix A of the vELC 1st EF-hand domain to be open constantly in all solutions; therefore the helix structure is broken by the A57G mutation. In addition to that, the A57G mutation

may exert its effect by disrupting the cross-bridge cycle, which is essential for the force generation.

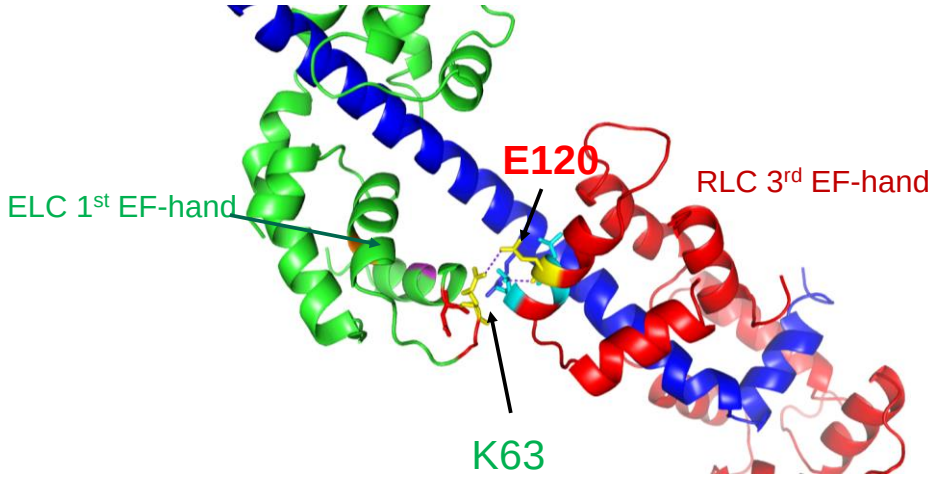

Figure 26 . Potential Salt-bridges and amino acid sequence comparison in the third loop area in RLC. The potential salt-bridge bets are between K63 in the N-terminal of vELC (green) and E120 in the C-terminal of vRLC (red)**.** The A57G, C81, K63 and E120 were depicted.

References

(2016/10/18/01:58:04). "NCBI CDD Conserved Protein Domain EFh." from https://www.ncbi.nlm.nih.gov/Structure/cdd/cddsrv.cgi?uid=cd00051 files/472/cddsrv.html.

Alberts, B., D. Bray, et al. (1994). Muscle. Molecular Biology of the Cell. New York, Garland Science.

Alberts, B., A. Johnson, et al. (2002). Glossary. Molecular Biology of the Cell. New York, Garland Science.

Andersen, P. S., P. L. Hedley, et al. (2012). "A novel Myosin essential light chain mutation causes hypertrophic cardiomyopathy with late onset and low expressivity." Biochemistry research international 2012: 685108.

Arad, M., M. Penas-Lado, et al. (2005). "Gene mutations in apical hypertrophic cardiomyopathy." Circulation 112(18): 2805-2811.

Bashyam, M. D., G. R. Savithri, et al. (2003). "Molecular genetics of familial hypertrophic cardiomyopathy (FHC)." Journal of Human Genetics 48(2): 55-64.

Bell, J. E. (1981). "Fluorescence: Solution Studies." Spectroscopy in Biochemistry 1(4): 155-194.

Dewey, T. G. (1991). Biophysical and biochemical aspects of fluorescence spectroscopy. New York, Plenum Press.

Dominguez, R., Y. Freyzon, et al. (1998). "Crystal structure of a vertebrate smooth muscle myosin motor domain and its complex with the essential light chain: Visualization of the pre-power stroke state." Cell 94(5): 559-571.

Eftink, M. R. (2000). "Use of fluorescence spectroscopy as thermodynamics tool." Energetics of Biological Macromolecules, Pt C 323: 459-473.

Eftink, M. R. and M. C. Shastry (1997). "Fluorescence methods for studying kinetics of protein-folding reactions." Methods in Enzymology 278: 258-286.

Fodor, W. L., B. Darras, et al. (1989). "Human ventricular/slow twitch myosin alkali light chain gene characterization, sequence, and chromosomal location." Journal of Biological Chemistry 264(4): 2143-2149.

Furtado, M. B., M. W. Costa, et al. (2016). "The cardiac fibroblast: Origin, identity and role in homeostasis and disease." Differentiation; research in biological diversity 92(3): 93-101.

Geeves, M. A. (2002). "Molecular motors: Stretching the lever-arm theory." Nature 415(6868): 129-131.

Geeves, M. A. and K. C. Holmes (2005). The Molecular Mechanism of Muscle Contraction. B. T. A. i. P. Chemistry, Academic Press. 71: 161-193.

Gulick, J., T. E. Hewett, et al. (1997). "Transgenic remodeling of the regulatory myosin light chains in the mammalian heart." Circulation Research 80(5): 655-664.

Hennecke, J., A. Sillen, et al. (1997). "Quenching of tryptophan fluorescence by the active-site disulfide bridge in the DsbA protein from Escherichia coli." Biochemistry 36(21): 6391-6400.

Hernandez, O. M., M. Jones, et al. (2007). "Myosin essential light chain in health and disease." American journal of physiology. Heart and circulatory physiology 292(4): H1643-1654.

Hernandez, O. M., M. Jones, et al. (2007). "Myosin essential light chain in health and disease." American Journal of Physiology - Heart and Circulatory Physiology 292(4): H1643-H1654.

Himmel, D. M., S. Mui, et al. (2009). "The On-Off Switch in Regulated Myosins: Different Triggers but Related Mechanisms." Journal of molecular biology 394(3): 496-505.

Houdusse, A. and C. Cohen (1996). "Structure of the regulatory domain of scallop myosin at 2 angstrom resolution: Implications for regulation." Structure 4(1): 21-32.

Huber, P. J., U. T. Brunner, et al. (1989). "Disulfide formation within the regulatory light chain of skeletal muscle myosin." Biochemistry 28(23): 9116-9123.

Kamm, K. E. and J. T. Stull (2011). "Signaling to Myosin Regulatory Light Chain in Sarcomeres." Journal of Biological Chemistry 286(12): 9941-9947.

Kawasaki, H. and R. H. Kretsinger (1994). "Calcium-binding proteins. 1: EF-hands." Protein profile 1(4): 343-517.

Kazmierczak, K., E. C. Paulino, et al. (2013). "Discrete effects of A57G-myosin essential light chain mutation associated with familial hypertrophic cardiomyopathy." American Journal of Physiology - Heart and Circulatory Physiology 305(4): H575-H589.

Kelly, R. and M. Buckingham (1997). "Manipulating Myosin Light Chain 2 Isoforms In Vivo." Circulation Research 80(5): 751-753.

Kitaoka, H., Y. Doi, et al. (2003). "Comparison of prevalence of apical hypertrophic cardiomyopathy in Japan and the United States." The American Journal of Cardiology 92(10): 1183-1186.

Knowles, A. C., R. E. Ferguson, et al. (2008). "Orientation of the essential light chain region of myosin in relaxed, active, and rigor muscle." Biophysical Journal 95(8): 3882-3891.

Konno, T., S. Chang, et al. (2010). "Genetics of Hypertrophic Cardiomyopathy." Current opinion in cardiology 25(3).

Lakowicz, J. R. (2006). Quenching of Fluorescence. Principles of Fluorescence Spectroscopy. J. R. Lakowicz, Springer US: 277-330.

Lee, W.-H., T. H. Hwang, et al. (2001). "Different expressivity of a ventricular essential myosin light chain gene Ala57Gly mutation in familial hypertrophic cardiomyopathy." American Heart Journal 141(2): 184-189.

Lodish, H., A. Berk, et al. (2000). Muscle: A Specialized Contractile Machine. New York, W. H. Freeman.

Lossie, J., D. S. Ushakov, et al. (2012). "Mutations of ventricular essential myosin light chain disturb myosin binding and sarcomeric sorting." Cardiovascular research 93(3): 390-396.

Lowey, S. and K. M. Trybus (1995). "Role of skeletal and smooth muscle myosin light chains." Biophysical Journal 68(4 Suppl): 120S-127S.

Maron, B. J. and M. S. Maron (2013). "Hypertrophic cardiomyopathy." The Lancet 381(9862): 242-255.

Maron, B. J., M. S. Maron, et al. (2012). "Genetics of Hypertrophic Cardiomyopathy After 20 YearsClinical Perspectives." Journal of the American College of Cardiology 60(8): 705-715.

Maron, B. J., W. J. McKenna, et al. (2003). "American College of Cardiology/European Society of Cardiology clinical expert consensus document on hypertrophic cardiomyopathy. A report of the American College of Cardiology Foundation Task Force on Clinical Expert Consensus Documents and the European Society of Cardiology Committee for Practice Guidelines." Journal of the American College of Cardiology 42(9): 1687-1713.

Mátyus, L., J. Szöllősi, et al. (2006). "Steady-state fluorescence quenching applications for studying protein structure and dynamics." Journal of Photochemistry and Photobiology B: Biology 83(3): 223-236.

Munishkina, L. A. and A. L. Fink (2007). "Fluorescence as a method to reveal structures and membrane-interactions of amyloidogenic proteins." Biochimica Et Biophysica Acta-Biomembranes 1768(8): 1862-1885.

Muthu, P., L. Wang, et al. (2011). "Structural and functional aspects of the myosin essential light chain in cardiac muscle contraction." The FASEB Journal 25(12): 4394-4405.

Ni, S., F. Hong, et al. (2012). "Modification of Interface between Regulatory and Essential Light Chains Hampers Phosphorylation-dependent Activation of Smooth Muscle Myosin." The Journal of Biological Chemistry 287(26): 22068-22079.

Olson, T. M., M. L. Karst, et al. (2002). "Myosin light chain mutation causes autosomal recessive cardiomyopathy with mid-cavitary hypertrophy and restrictive physiology." Circulation 105(20): 2337-2340.

Potter, J. D. (1982). [22] Preparation of troponin and its subnits. B. T. M. i. Enzymology, Academic Press. 85: 241-263.

Rayment, I., W. R. Rypniewski, et al. (1993). "Three-dimensional structure of myosin subfragment-1: a molecular motor." Science 261(5117): 50-58.

Richard, P., P. Charron, et al. (2003). "Hypertrophic cardiomyopathy: distribution of disease genes, spectrum of mutations, and implications for a molecular diagnosis strategy." Circulation 107(17): 2227-2232.

Richard, P., P. Charron, et al. (2003). "Hypertrophic cardiomyopathy: distribution of disease genes, spectrum of mutations, and implications for a molecular diagnosis strategy." Circulation 107(17): 2227-2232.

Roopnarine, O. (2003). "Mechanical Defects of Muscle Fibers with Myosin Light Chain Mutants that Cause Cardiomyopathy." Biophysical Journal 84(4): 2440-2449.

Roopnarine, O. and R. J. Price (2014). "Time-Resolved Fluorescence Quenching Measurements to Study the Structural Defects Induced by Myosin Essential Light Chain Cardiomyopathy Mutations in Muscle Fibers." Biophysical Journal 106(2): 162a-162a.

Roopnarine, O., A. G. Szent-Györgyi, et al. (1998). "Microsecond Rotational Dynamics of Spin-Labeled Myosin Regulatory Light Chain Induced by Relaxation and Contraction of Scallop Muscle." Biochemistry 37(41): 14428-14436.

Schaub, M. C., M. A. Hefti, et al. (1998). "Modulation of contractility in human cardiac hypertrophy by myosin essential light chain isoforms." Cardiovascular research 37(2): 381-404.

Sellers, J. R., P. D. Chantler, et al. (1980). "Hybrid Formation between Scallop Myofibrils and Foreign Regulatory Light-Chains." Journal of molecular biology 144(3): 223-245.

Serrano, L., J. L. Neira, et al. (1992). "Effect of Alanine Versus Glycine in Alpha-Helices on Protein Stability." Nature 356(6368): 453-455.

Sillen, A. and Y. Engelborghs (1998). "The correct use of "average" fluorescence parameters." Photochemistry and Photobiology 67(5): 475-486.

Spudich, J. A. (2014). "Hypertrophic and dilated cardiomyopathy: four decades of basic research on muscle lead to potential therapeutic approaches to these devastating genetic diseases." Biophysical Journal 106(6): 1236-1249.

Sutoh, K. (1982). "An actin-binding site on the 20K fragment of myosin subfragment 1." Biochemistry 21(19): 4800-4804.

Sweeney, H. L., B. F. Bowman, et al. (1993). "Myosin light chain phosphorylation in vertebrate striated muscle: regulation and function." The American journal of physiology 264(5 Pt 1): C1085-1095.

Sweeney, H. L. and A. Houdusse (2010). "Structural and Functional Insights into the Myosin Motor Mechanism." Annual Review of Biophysics 39(1): 539-557.

Szczesna-Cordary, D., G. Guzman, et al. (2004). "Familial Hypertrophic Cardiomyopathy-linked Alterations in Ca2+ Binding of Human Cardiac Myosin Regulatory Light Chain Affect Cardiac Muscle Contraction." Journal of Biological Chemistry 279(5): 3535-3542.

Szczesna, D. (2003). "Regulatory light chains of striated muscle myosin. Structure, function and malfunction." Current drug targets. Cardiovascular & haematological disorders 3(2): 187-197.

Szczesna, D., J. Zhao, et al. (1996). "The regulatory light chains of myosin modulate cross-bridge cycling in skeletal muscle." The Journal of Biological Chemistry 271(9): 5246-5250.

Szymanski, M. R., M. J. Jezewska, et al. (2013). "Energetics of the Escherichia coli DnaT Protein Trimerization Reaction." Biochemistry 52(11): 1858-1873.

Tardiff, J. C. (2005). "Sarcomeric Proteins and Familial Hypertrophic Cardiomyopathy: Linking Mutations in Structural Proteins to Complex Cardiovascular Phenotypes." Heart Failure Reviews 10(3): 237-248.

Taylor, K. A., M. Feig, et al. (2014). "Role of the essential light chain in the activation of smooth muscle myosin by regulatory light chain phosphorylation." Journal of structural biology 185(3): 375-382.

Ushakov, D. S., V. Caorsi, et al. (2011). "Response of rigor cross-bridges to stretch detected by fluorescence lifetime imaging microscopy of myosin essential light chain in skeletal muscle fibers." The Journal of Biological Chemistry 286(1): 842-850.

Vikstrom, K. L. and L. A. Leinwand (1996). "Contractile protein mutations and heart disease." Current opinion in cell biology 8(1): 97-105.

Wagner, P. D. (1982). "Preparation and fractionation of myosin light chains and exchange of the essential light chains." Methods in Enzymology 85 Pt B: 72-81.

Wagner, P. D. and A. G. Weeds (1977). "Studies on the role of myosin alkali light chains. Recombination and hybridization of light chains and heavy chains in subfragment-1 preparations." Journal of molecular biology 109(3): 455-470.

Wang, Y., Y. Xu, et al. (2006). "Prolonged Ca2+ and force transients in myosin RLC transgenic mouse fibers expressing malignant and benign FHC mutations." Journal of molecular biology 361(2): 286-299.

Watkins, H., A. Rosenzweig, et al. (1992). "Characteristics and Prognostic Implications of Myosin Missense Mutations in Familial Hypertrophic Cardiomyopathy." New England Journal of Medicine 326(17): 1108-1114.

Watterson, J. G., L. Kohler, et al. (1979). "Evidence for two distinct affinities in the binding of divalent metal ions to myosin." The Journal of Biological Chemistry 254(14): 6470-6477.

Willott, R. H., A. V. Gomes, et al. (2010). "Mutations in Troponin that cause HCM, DCM AND RCM: What can we learn about thin filament function?" Journal of Molecular and Cellular Cardiology 48(5): 882-892.

Xie, X., D. H. Harrison, et al. (1994). "Structure of the Regulatory Domain of Scallop Myosin at 2.8 Angstrom Resolution." Nature 368(6469): 306-312.

Zoghbi, M. E., J. L. Woodhead, et al. (2008). "Three-dimensional structure of vertebrate cardiac muscle myosin filaments." Proceedings of the National Academy of Sciences of the United States of America 105(7): 2386-2390.